Title
Summertime partitioning and budget of NO_ycompounds in the troposphere over Alaska and Canada: ABLE 3B

Journal
Journal of Geophysical Research, 99(D1)

ISSN
0148-0227

Authors
Sandholm, S
Olson, J
Bradshaw, J
et al.

Publication Date
1994-01-20

DOI
10.1029/93jd02458

JOURNAL OF GEOPHYSICAL RESEARCH, VOL. 99, NO. D1, PAGES 1837–1861, JANUARY 20, 1994

Summertime partitioning and budget of NO_y compounds in the troposphere over Alaska and Canada: ABLE 3B

S. Sandholm,[1] J. Olson,[1] J. Bradshaw,[1] R. Talbot,[2] H. Singh,[3] G. Gregory,[4] D. Blake,[5] B. Anderson,[4] G. Sachse,[4] J. Barrick,[4] J. Collins,[4] K. Klemm,[2,6] B. Lefer,[2] O. Klemm,[2,6] K. Gorzelska,[2] D. Herlth,[3] and D. O'Hara[3]

As part of NASA's Arctic Boundary Layer Expedition 3A and 3B field measurement programs, measurements of NO_x, HNO_3, PAN, PPN, and NO_y were made in the middle to lower troposphere over Alaska and Canada during the summers of 1988 and 1990. These measurements are used to assess the degree of closure within the reactive odd nitrogen (N_xO_y) budget through the comparison of the values of NO_y measured with a catalytic convertor to the sum of individually measured $NO_y(i)$ compounds (i.e., $\Sigma NO_y(i) = NO_x + HNO_3 + PAN + PPN$). Significant differences were observed between the various study regions. In the lower 6 km of the troposphere over Alaska and the Hudson Bay lowlands of Canada a significant fraction of the NO_y budget (30 to 60%) could not be accounted for by the measured $\Sigma NO_y(i)$. This deficit in the NO_y budget is about 100 to 200 parts per trillion by volume (pptv) in the lower troposphere (0.15 to 3 km) and about 200 to 400 pptv in the middle free troposphere (3 to 6.2 km). Conversely, the NO_y budget in the northern Labrador and Quebec regions of Canada is almost totally accounted for within the combined measurement uncertainties of NO_y and the various $NO_y(i)$ compounds. A substantial portion of the NO_y budget's "missing compounds" appears to be coupled to the photochemical and/or dynamical parameters influencing the tropospheric oxidative potential over these regions. A combination of factors are suggested as the causes for the variability observed in the NO_y budget. In addition, the apparent stability of compounds represented by the NO_y budget deficit in the lower-altitude range questions the ability of these compounds to participate as reversible reservoirs for "active" odd nitrogen and suggest that some portion of the NO_y budget may consist of relatively unreactive nitrogen-containing compounds.

1. Introduction

In many regions of the remote troposphere the availability of reactive odd nitrogen in the form of nitric oxide (NO) is a critical factor controlling the photochemical production of ozone (O_3) . This control of O_3 production occurs through NO reaction with hydroperoxy and organoperoxy radicals (HO_2 and RO_2). The photochemical destruction rate for O_3 is believed to be controlled by reactions of O_3 with the hydroperoxy radical (HO_2) and by direct photolysis of O_3 leading to hydroxyl radical (OH) production. The absence of NO would result in a net photochemical loss of O_3 throughout the troposphere. Over remote tropical and midlatitude marine environments, observed NO mixing ratios have been small enough (i.e., NO mixing ratios of a few parts per trillion by volume) to yield predictions of net ozone loss throughout most of the middle to lower troposphere in these locations [e.g., *Liu et al.*, 1983; *Chameides et al.*, 1987; *Carroll et al.*; 1990]. The NO mixing ratios observed in the summertime troposphere (0.15 - 6.2 km) over Alaska were, on average, slightly larger than those observed over the remote lower-latitude marine environments [*Sandholm et al.*, 1992]. The summertime NO mixing ratios over Alaska were still small enough to result in predictions of a net photochemical loss of O_3 in the lower 6-km column. In these cases the O_3 photochemical lifetime was predicted to be nearly equal to the lifetime based on surface deposition. These results also indicated that the O_3 photochemical lifetime was nearly 2.5 times longer than that predicted in the absence of NO [*Jacob et al.*, 1992]. The middle to lower tropospheric summertime measurements of NO made over the Arctic and subarctic regions of both Alaska and Canada fall within the range of mixing ratios (i.e., NO < 200 pptv [*Sandholm et al.*, 1992; *Talbot et al.*, this issue]) that have been characterized as NO-limited environments with regard to production of the oxidants OH and O_3 [cf. *Logan et al.*, 1981; *Lin et al.*, 1988; *Hough and Johnson*, 1991; *Chameides et al.*, 1992].

Control of NO mixing ratios on the few minutes timescale is exerted via the fast photochemical cycle involving NO reactions with O_3 and peroxyradicals that lead to the formation of nitrogen dioxide (NO_2) and NO's subsequent reformation via the photolysis of NO_2. Permanent loss of tropospheric NO is believed to be dominated by the loss of NO_2 through the formation of nitric acid (HNO_3) via reactions such as $OH + NO_2 (+ M) \rightarrow HNO_3$. This latter reaction is sufficiently fast in the

[1]School of Earth and Atmospheric Sciences, Georgia Institute of Technology, Atlanta.
[2]Institute for the Study of Earth, Oceans, and Space, University of New Hampshire, Durham.
[3]NASA Ames Research Center, Moffett Field, California.
[4]NASA Langley Research Center, Hampton, Virginia.
[5]Department of Chemistry, University of California at Irvine.
[6]Now at Fraunhofer-Institut für Atmosphärische Umweltforschung, Garmisch-Partenkirchen, Germany.

Paper number 93JD02458.
0148-0227/93/93JD-02458$05.00

summertime lower troposphere (of the order of hours) to significantly deplete both NO and NO_2 (NO + NO_2 = NO_x) from air parcels within a few days travel time of their NO_x sources [e.g., *Logan,* 1983].

In contrast to the loss of NO_x represented above by the HNO_3 sink, NO_x can be converted to a number of stable reservoir compounds such as pernitric acid (HO_2NO_2), peroxyacetyl nitrate (PAN), and various other alkyl nitrates ($RONO_2$) and NO_x-containing hydrocarbons. These reservoir compounds can act to transport the NO_x pool over large distances [e.g., *Crutzen,* 1979; *Logan et al.,* 1981; *Singh and Hanst,* 1981; *Singh,* 1987], and collectively form the dominant component of the "active" odd nitrogen family in some regions of the remote troposphere. Observations made in the middle to lower summertime troposphere over Alaska have indicated that under certain conditions the thermal decomposition of PAN alone could account for the NO_x abundance in the lower 6-km tropospheric column [*Singh et al.,* 1992*b*], whereas in other cases the middle tropospheric (4 - 6 km) abundance of NO_x may have been controlled by the degradation of other NO_x reservoir compounds [*Jacob et al.,* 1992].

The active odd nitrogen compounds discussed above represent a subset of the larger pool of total atmospheric odd nitrogen (N_xO_y), which includes more stable compounds such as HNO_3 and particulate nitrate ($p\text{-}NO_3^-$) that are not currently believed to be readily converted back into NO_x under typical middle to lower tropospheric conditions. Measurement of total odd nitrogen (N_xO_y) is possible using the analytical techniques based on the catalytic reduction of N_xO_y compounds to NO [*Bollinger et al.,* 1983; and *Fahey et al.,* 1986]. Several studies have shown that the "total" odd nitrogen compounds measured by this technique (NO_y) is often greater than the sum of the subset of individually measurable, $NO_y(i)$, odd nitrogen compounds (e.g., $NO_y > \Sigma NO_y(i)$ [*Fahey et al.,* 1986; *Ridley,* 1991; *Singh et al.,* 1992; *Atlas et al.,* 1992]). In these studies the subset of individually measured $NO_y(i)$ compounds was initially believed to represent the bulk of the anticipated N_xO_y family members with the list of measured $NO_y(i)$ compounds increasing in progressive studies [e.g., *Atlas et al.,* 1992; *Buhr et al.,* 1990]. The unidentified N_xO_y compounds that are implied from the deficit found in $NO_y - \Sigma NO_y(i)$ may serve as reservoirs for the transport of active odd nitrogen into the remote troposphere [*Fahey et al.,* 1986; *Singh,* 1987; *Roberts,* 1990; *Buhr et al.,* 1990; *Jacob et al.,* 1992]. Further characterization of the distribution and magnitude of the known and implied unknown components of the active odd nitrogen reservoir is important to the understanding of the factors controlling the abundance of NO_x in remote regions.

The characterization of high northern latitude middle to lower tropospheric trace gas distributions was one goal of the NASA Global Tropospheric Experiment (GTE) Artic Boundary Layer Expedition (ABLE) phase 3 programs. The airborne sampling portions of these programs surveyed the trace gas distributions over Alaska in the summer of 1988 (ABLE 3A) [e.g., *Harriss et al.,* 1992] and the Hudson Bay lowlands and northeastern boreal forest of Canada in the summer of 1990 (ABLE 3B) [e.g., *Harriss et al.,* this issue]. A wide range of chemical and physical variables were measured during these programs, including NO, NO_2, PAN, PPN, HNO_3, $p\text{-}NO_3^-$, NO_y, O_3, CO, CH_4, nonmethane hydrocarbons (NMHCs), C_2Cl_4, and H_2O.

This suite of measurements provides a unique opportunity to study the summertime partitioning of active and reservoir odd nitrogen compounds in the middle to lower tropospheric air masses overlying remote regions of the high-latitude continent of North America. In this paper we examine the partitioning of individual odd nitrogen compounds within the measured N_xO_y budget and address issues related to the budget's degree of closure and its relationship with other physical, chemical, and measurement-related variables. Details of the distribution and relationship of odd nitrogen compounds and other trace gases are described in a series of papers presented in the *Journal of Geophysical Research* special issue for ABLE 3A and in this issue. The entire NASA/GTE ABLE 3 data archive is available from the NASA/GTE project office (Langley, Virginia).

2. MEASUREMENT INSTRUMENTATION

Both the ABLE 3A (Alaskan) and the ABLE 3B (Canadian) airborne field programs were conducted on the NASA Wallops Flight Facility L-188 Electra aircraft. Although some modification of each N_xO_y instrument occurred between the 1988 ABLE 3A and the 1990 ABLE 3B programs, the fundamental measurement methodology underlying each instrument was identical for the two programs. Details of the $NO_y(i)$ and NO_y measurement techniques are discussed in sections 2.1 through 2.4. The techniques used for concurrent measurements of O_3, CO, selected nonmethane hydrocarbons, and meteorological variables have been described elsewhere [*Gregory et al.,* 1983; *Sachse et al.,* 1987; *Blake et al.,* 1992; *Harriss et al.,* this issue].

2.1. *NO_x and NO_y Measurements*

The spectroscopically selective two-photon/laser-induced fluorescence (TP/LIF) NO technique was applied to the simultaneous measurement of NO, NO_2, and NO_y. Details of this instrument have been previously reported [*Bradshaw et al.,* 1985; *Sandholm et al.,* 1990; *Sandholm et al.,* 1992]. The 226-nm and 1.1-μm laser beams used in the two-photon fluorescence excitation process were passed through three separate ambient sampling cells. One cell was designated for detecting ambient NO. A second cell was designated for detecting NO produced from a photolytic conversion of ambient NO_2. The third cell was designated for detecting NO produced from the 300°C gold-catalyzed conversion of ambient NO_y using 0.3% CO as a reducing agent. The NO, NO_2, and NO_y channels

used separate signal acquisition electronics, flow measurement and control systems, and signal normalization/internal reference standards.

Ambient air was continuously drawn in through a common porcelain-glass coated inlet (2.5-cm ID) at a nominal flow rate of 200 liters per minute (lpm). The airstream was sampled perpendicular to the aircraft motion. The sample residence time through the inlet manifold was always less than half a second. Total sample residence time through the NO ambient sampling portion of the instrument was less than 1 s. Sample residence time in the NO_2 portion of the instrument varied between 1 and 5 s, depending on the photolytic converter system used. NO_y samples were drawn from the center of the ambient sampling manifold at a location near the NO_y converter assembly with a residence time < 0.2 s from the manifold to the NO_y converter. The sampling manifold and flow line fittings were tested inflight for leaks using a 10 parts per million by volume (ppmv) NO standard as a leak tracer.

During ABLE 3A an excimer laser was used as the photolytic convertor system's photolysis source [*Sandholm et al.*, 1990; *Sandholm et al.*, 1992]. To reduce the instrument's size, weight, and power consumption, a high-pressure xenon arc-lamp-based photolytic converter was used during the ABLE 3B program. This latter converter utilized a 1-kW Cermax short-arc lamp that was spectrally filtered into a photolysis passband of 350 nm < λ < 420 nm. This converter was designed to operate at 30% to 60% photolytic efficiency with sample residence times ranging from 2 to 4.5 s, respectively. The low wavelength cutoff (10% peak spectral fluence) of 350 nm was chosen to minimize possible interferences from concomitant R-NO_x compounds. Deep UV (λ < 330 nm) and Visible/IR (λ > 480 nm) emissions from the lamp were attenuated by > 10^3-fold relative to the intensity at the center of the passband. The photolysis beam was also spatially filtered to avoid illumination of the photolytic sample cell's walls. In both the excimer laser and the arc-lamp-based converters, the photolytic sample cells were thermally controlled using a high flow rate of ambient air that was passed through an outer jacket of each cell.

The NO_y catalytic converter system used with the TP/LIF sensor was adapted from the NO_y converter system design developed by NOAA [*Bollinger et al.*, 1983; *Fahey et al.*, 1985; *Murphy* and *Fahey*, 1987]. In the ABLE 3A program a short length (~ 0.3 m) of PFA Teflon tubing was used to connect the NO_y converter to the main porcelain-glass-coated sampling manifold. This tubing was replaced by a similar length of heated (~40°C) gold-coated nickel tubing in the ABLE 3B program. This change was made to minimize the possible effects of sample line memory during the more rapid descents/ascents planned for the ABLE 3B field program. During the 1989 NASA/GTE Chemical Instrumentation Test and Evaluation (CITE) 3 field program a similar PFA Teflon tubing was used to couple the NO_y convertor to the inlet/manifold. In this latter case, a positive artifact was believed to have been induced by sample line memory effects following the rapid descent (500 m/min) through haze layers that occurred near the trade wind inversion over the equatorial western Atlantic Ocean near Natal, Brazil.

Inflight and preflight/postflight calibrations were performed by standard additions to either ambient air (inflight) or bottled air (preflight/postflight). Two-stage serial dilution systems were used to dilute the parts per minute by volume mixing ratios of standards contained by high-pressure aluminum cylinders. The diluted standards were injected directly into the ambient sampling inlet and subsequently diluted to final concentration (0.1 to 2 parts per billion by volume (ppbv)). All flow measurements were made with linear mass flow controllers or meters. These devices were intercompared with positive volume displacement flow measurement instrumentation prior to and after both the ABLE 3A and ABLE 3B field programs.

Primary and secondary gas calibration standards were used for both NO and NO_2. The 50 ppmv (in nitrogen) NO and NO_2 primary standards used for intercalibration have remained stable since their acquisition in 1981 (i.e., < 10% deviation from initial conditions from 1981 to 1991). Standards were intercompared with National Institute of Standards and Technology (NIST) standards as part of the NASA/GTE field measurement program protocol in 1983, 1984, 1986, 1990, and 1991. High-pressure nitroethane ($C_2H_5NO_2$) in helium standards were developed to provide a more rigorous test of the NO_y conversion efficiency. These $C_2H_5NO_2$ standards were made from reagent grade $C_2H_5NO_2$ that was further purified by several low-temperature vacuum distillations in which only the middle third of the distillate was retained. Aluminum cylinders were vacuum baked (< 10^{-3} mbar, 50°C) and flushed several times, then filled with a known pressure of the purified $C_2H_5NO_2$ and diluted with research purity helium to a final cylinder pressure of about 1600 psig. Final $C_2H_5NO_2$ mixing ratios determined from the cylinder contents by UV absorption agreed to within 10% of the value calculated from partial pressure dilution. The $C_2H_5NO_2$ standards have proven to be stable at mixing ratios in the range of 10 ppmv. Inflight calibrations were made using NO and NO_2 during ABLE 3A and using NO, NO_2, and $C_2H_5NO_2$ during ABLE 3B.

The preflight/postflight mixing ratios measured in bottled air to which no standard was added were not subtracted as "blank" values for the NO_x or NO_y measurements reported here. We believe these "blank" values, which ranged from approximately 40 to 120 pptv, predominantly reflected outgassing, under slow flow conditions (≤ 40 slpm), of the long length of extra tubing (~15 m) used to reach the aircraft inlet. This belief is based on decay of signal versus time that typically indicated approximately 1 to 2 hours for this system to "clean" up and approach the lower end of the range of mixing ratios stated above. The instrument's background was continuously monitored by blocking of the 1.1-μm laser beam at a frequency of 1 Hz and by periodically tuning the

226-nm laser's wavelength off of a NO resonant transition. Significant systematic changes were not detected in the numerous zero checks, calibrations, and converter efficiency tests of the NO_y instrument, except for one noticeable reduction in the conversion efficiency for $C_2H_5NO_2$ (0.96 to 0.75). This decrease occurred after sampling a smelter plume during the ABLE 3B return transit flights on mission 21. Subsequent NO_y measurements taken during the remainder of transit flights (missions 21 and 22) were reported as lower limits, and these data have not been used in this study.

The calibrations used to derive each flight's ambient NO, NO_2, and NO_y mixing ratios had, at the 95% confidence limit, standard deviations about the mean of ±16%, ±18%, and ±18%, respectively. The limit of detection (LOD) for a signal-to-noise ratio of 2/1 averaged 2 pptv for NO and 6 pptv for NO_2 using a 3-min signal integration time. The photon statistics based measurement precision at the 95% confidence limit (3 minutes integration) was typically ±25% for NO = 15 pptv, ±35% for NO_2 = 35 pptv, and ±8.5% for NO_y = 700 pptv. Measurement precision was proportional to the square root of mixing ratio and/or integration time.

The TP/LIF NO technique was used in both the NASA/GTE CITE 1 (1983) and the CITE 2 (1984) airborne intercomparison programs [*Hoell et al.*, 1987; *Gregory et al.*, 1990*a*]. These intercomparisons concluded that at low mixing ratios (i.e., < 60 pptv), NO measurements agreed with the stated instruments' precision and accuracy. The level of agreement among instruments was of the order of 35%. On average, individual measurements agreed within 5 to 7 pptv for NO mixing ratios of < 20 pptv. Concurrently, the photofragmentation TP/LIF NO_2 technique was evaluated during the CITE 2 airborne intercomparison program [*Gregory et al.*, 1990*b*]. The NO_2 intercomparison study also concluded that, on average, the NO_2 measurements agreed within the stated instrument precision and accuracy at low NO_2 mixing ratios (i.e., NO_2 < 200 pptv). Individual measurements showed a 30 to 40% level of agreement (i.e., 15 to 20% from the average). Intercomparison at the lowest NO_2 mixing ratios (i.e., NO_2 < 50 pptv) revealed individual measurements were uncorrelated due to the randomness associated with approaching the instruments' limits of detection. On average, NO_2 values still agreed within the instruments' stated accuracy [*Gregory et al.*, 1990*a,b*]. The instruments used in the ABLE 3A and ABLE 3B field programs were nearly identical in their evaluated precision and accuracy for NO and NO_2.

2.2. *Peroxyacetyl Nitrate (PAN), Peroxypropionyl Nitrate (PPN) Measurements*

PAN and PPN were measured using a cryotrap (CT) preconcentration sample loop in conjunction with gas chromatographic (GC) separation, and a tandem columetric electron capture detection (ECD system). In the CT/GC/ECD technique, typically 0.10 to 0.20 standard liters of ambient air, drawn through an aft-facing Teflon inlet, were enriched in a cryotrap held at a constant -150° C temperature. The preconcentrated samples were then analyzed using a GC/ECD that was operated at constant pressure (1050 mbar).

Calibration of the PAN instrument was accomplished using diffusion tubes containing PAN standards that were prepared by the $CH_3CHO/NO_2/Cl_2$ photolysis method [*Singh and Salas*, 1983] and dissolved/stored in liquid n-tridecane [*Gaffney et al.*, 1984]. Air was passed over the diffusion tube at a constant rate of flow to provide a calibration gas stream having PAN mixing ratios in the ppbv range. This calibration gas stream was periodically added at a downstream point in the ambient sampling line. PAN mixing ratios in the calibration gas stream were measured onboard the aircraft using a hot molybdenum oxide converter (375°C) coupled to a chemiluminescence NO monitor. Calibration of this chemiluminescence system was accomplished using both NO_2 and NO standards that were intercompared with NIST primary standards as part of the CITE 2 and ABLE 3B field program protocols. The calibration gas stream was further diluted using a two-stage serial dilution system to provide final PAN calibration mixing ratios in the parts per trillion by volume range. Linear mass flow controllers/meters used in this dilution system were compared with volume displacement standards. The accuracy of the PAN calibration transfer to ambient air measurements is estimated to be ±25% at the 95% confidence level.

The CT/GC/ECD PAN instrument was shown to be linear for PAN mixing ratios ranging from 5 to 1000 pptv. The typical limit of detection of the CT/GC/ECD PAN instrument was < 5 pptv for 100 ml of sampled air. Measurement precision was ±10% at the 95% confidence level for PAN mixing ratios that were well above the limit of detection (i.e., PAN ≥ 50 pptv).

This CT/GC/ECD PAN instrument was used in the NASA/GTE CITE 2 airborne intercomparison program [*Gregory et al.*, 1990c]. This intercomparison program pointed out the need for onboard verification of PAN standards. As outlined above, onboard PAN standard verification was carried out during both ABLE 3A and ABLE 3B. The CITE 2 airborne intercomparison concluded that the two PAN instruments agreed, on the average, to about 20 pptv for PAN mixing ratios < 100 pptv. At larger PAN mixing ratios, agreement between individual measurements and the average was possible at the ±30% level for a 95% confidence limit even though individual pairs of measurements might sometimes fall outside this range. The PAN measurements that were intercompared fell close to agreeing within the stated accuracy and precision of the instruments [*Gregory et al.*, 1990*c*].

2.3. *HNO_3 Measurements*

Gas phase HNO_3 was measured using a mist-chamber (MC) aqueous scrubber as a preconcentrator for subsequent determination of NO_3^- by ion chromatography

(IC). Details of this technique have been previously described [*Talbot et al.*, 1990; *Talbot et al.*, 1992]. In this technique, gas phase HNO_3 and other soluble gases were stripped from ambient air into a dense mist of ultrapure deionized water. The mist was collected on a Teflon filter that recirculated the mist chamber's water supply to the pneumatic nebulizer that formed the mist. A Teflon prefilter was installed in the sampling line, upstream of the mist chamber, in order to segregate against the collection of water soluble particulate-nitrate ($p\text{-}NO_3^-$). The mist chamber sampled ambient air at a flow rate of 30 to 40 standard liters per minute (slpm) from a main ambient sampling manifold and inlet system that drew in approximately 300 slpm of ambient air. All flow rates were measured with linear mass flow meters that were calibrated prior to and after each field program. A Teflon-coated inlet/sampling manifold was used during the ABLE 3A field program, whereas a 40-mm ID porcelain-glass-coated inlet/sampling manifold was used during the ABLE 3B program. This latter inlet/sampling manifold was nearly identical to the design used by the NO_x/NO_y instrument described previously. Laboratory tests of the porcelain-glass-coated inlet/manifold demonstrated 100 (±3)% passing efficiency for HNO_3 mixing ratios in the 100-300 pptv range using flow rates of approximately 300 slpm. The change of inlet/manifold coating materials was prompted by concerns over possible sampling memory effects from a Teflon-coated system. HNO_3 passing efficiency of the 25-mm ID Teflon-coated inlet used in ABLE 3A averaged 80% to 85% [*Talbot et al.*, 1992*a*]. HNO_3 mixing ratios reported for the ABLE-3A program were corrected for a passing efficiency of 80%.

The MC/IC calibrations were based on solutions prepared from dried KNO_3. These nitrate standards have agreed within ±3% of NIST standard solutions. The IC limit of detection (LOD) for HNO_3 was equivalent to 20 pptv for a 30-min sample collection time, using 30 slpm sample flow rates, where the LOD is inversely proportional to changes in the sample collection time. Blanks were obtained prior to each flight by sampling ambient air that was scrubbed of HNO_3 after passing through a series of impregnated and activated charcoal filters. Blank values were consistently at or below the LOD of the IC system using a 30-min sample collection time. Accuracy of the ICs calibration transfer to ambient HNO_3 measurements is estimated to be ±20% at the 95% confidence level, based on the uncertainties in the IC analysis of NO_3^-, the results of laboratory tests of the MC's collection and the inlet's passing efficiencies for HNO_3, and the uncertainties in the measurement of the sampled air volume. The sampling time used during ABLE 3A ranged from 15 minutes to 3 hours, whereas those used during the ABLE-3B program ranged from 3 to 45 minutes.

The MC/IC technique has yet to participate in an airborne intercomparison study. The MC/IC technique has been used in a recent ground-based HNO_3 intercomparison. The HNO_3 measurement techniques used in this ground-based intercomparison included the MC/IC technique discussed here, a NOAA nylon filter collection technique, and a continuous flow liquid diffusion scrubber (preconcentrator) based system developed by Lind at NCAR. In all three techniques, ion chromatography was used to measure the NO_3^- that was collected by the preconcentrators. The preliminary results of this intercomparison indicated that on average the individual techniques agreed within ±25% of the mean value formed between pairs of measurements over the HNO_3 mixing ratio range of 100 pptv to 500 pptv. Even so, individual pairs of HNO_3 measurements fell outside this range (E. L. Atlas et al., An intercomparison of three HNO_3 measurement techniques, submitted to *Journal of Geophysical Research*, 1992).

2.4. *Particulate NO_3^- Measurements*

Particulate NO_3^- ($p\text{-}NO_3^-$) was measured using an isokinetic aerosol sampling probe with a curved-leading edge nozzle design [*Talbot et al.*, 1992*a,b*]. A shrouded version of this nozzle design was used during the ABLE 3B field program. The collection efficiency of supermicron particles was greater than that for equivalent inlets using a sharp-leading edge nozzle design similar to those evaluated by *Hubert et al.* [1990]. Even so, the collection efficiency for supermicron particles must still be considered as uncertain. For submicron particles the curved leading edge nozzle has been shown to give significantly larger passing efficiency than straight edge designs with minimal loss on the nozzle inlet or curved tube sampling manifold wall (R. W. Talbot et al., Improvements in aerosol inlet performance in airborne applications, submitted to Journal of Atmospheric and Oceanographic Technology, 1992).

The Teflon 90-mm filters were mounted on supports made of Delrin and contained by a Delrin housing. Particles were collected on a stacked set of Nuclepore (8 μm) and Zefluor (1 μm) filters during the ABLE 3A program, whereas a single Zefluor (2 μm) filter arrangement was used in the ABLE 3B program. Sample collection times ranged from 15 minutes to 2 hours using a nominal ambient airflow rate of 475 lpm. These filter samples were analyzed for soluble NO_3^- by ionchromatography.

Filter blanks for $p\text{-}NO_3^-$ were equivalent to ambient mixing ratios of 4 pptv and were subtracted from reported values. The accuracy of the ambient air equivalent NO_3^- that was measured on the filters was estimated to be ±20% at the 95% confidence level, excluding uncertainties involving the sample inlet passing/collection efficiency.

Some fraction of fine $p\text{-}NO_3^-$ - containing aerosols was most likely collected and converted in the NO_y system. This fraction is believed to be significantly smaller than that collected by the curved leading edge aerosol sampling system. Even though there is some degree of uncertainty on an absolute scale, the $p\text{-}NO_3^-$ measurements that were made by the curved leading edge sampler described here should allow for an examination of relative trends in fine $p\text{-}NO_3^-$, with respect to closure of the measured N_xO_y family budget.

3. Results and Discussion

3.1. *Air Mass Characteristics*

The Alaskan portion of the ABLE 3A program (missions 6-26) primarily overflew study regions near Barrow and Bethel, Alaska. Air masses encountered in the ABLE 3A program originated from regions that were typically free from anthropogenic sources based on 3- to 5-day air mass back-trajectory analyses. These air mass origins were determined to be from two primary source regions, namely, the Gulf of Alaska/Bering Sea, and northern Siberia/Arctic packice. Missions 14-21 were characterized by air masses originating from the Gulf of Alaska and Bering Sea, whereas missions 6-13 and 24-26 were characterized by air masses originating over northern Siberia and the Arctic packice [*Shipham et al.*, 1992]. In general, the air masses sampled over Alaska had chemical signatures that suggested inputs of upper tropospheric to lower stratospheric air, biomass burning emissions from Alaska and Siberia, and longer-range transport of anthropogenic emissions from both Siberian and midlatitude Euro-Asian sources [*Sandholm et al.*, 1992; *Jacob et al.*, 1992; *Wofsy et al.*, 1992].

The ABLE 3B program focused on two primary study areas, the Hudson Bay lowlands over northern Ontario/Manitoba (missions 2-9) and the boreal-forested regions of northern Labrador and Quebec (missions 11-19). The air mass origins for these study areas, based on 3- to 5-day back-trajectory analyses, depicted a wide range of source regions that varied as the polar jet migrated between approximately 52° N and 66° N [*Shipham et al.*, this issue]. The air masses sampled over the Hudson Bay lowlands generally originated from Alaska and the Northwest Territories. These air masses possessed chemical signatures that suggest inputs of upper tropospheric to lower stratospheric air and air influenced by biomass burning in western Canada and Alaska [*Talbot et al.*, this issue; *Anderson et al.*, this issue; *Shipham et al.*, this issue].

Air masses sampled over the northern Quebec/Labrador region appeared to have a mixture of source influences. Biomass burning inputs were most notable on missions 11 and 13. In sharp contrast, several air masses encountered on missions 14-19 possessed chemical signatures similar to what could be characterized as tropical air. These tropical air masses are believed to have been remnants of tropical Pacific air in association with Typhoon Steve and with remnants of tropical Atlantic air in association with Hurricane Bertha [*Anderson et al.*, this issue; *Blake et al.*, this issue; *Shipham et al.*, this issue]. In addition to these tropically influenced air masses, air masses with characteristics of upper tropospheric to lower stratospheric origin were also encountered, most notably on missions 15-19 [*Talbot et al.*, this issue; *Browell et al.*, this issue]. In general, only the transit flight from Ontario to Labrador (mission 10) and a low-altitude flight leg over the Atlantic Ocean (mission 16) exhibited evidence of anthropogenic inputs from midlatitude sources in association with a strong southerly airflow.

3.2. *N_xO_y Measurements*

The various NO_y(i) measurements made during the ABLE 3 field programs covered a wide range of sampling time intervals. The HNO_3 (and p-NO_3^-) measurement system used the longest sampling/preconcentration times with sampling times, which ranged from 3 min to 3 hours and covered spatial scales from about 25 km to 500 km. In general, the sampling times of this instrument were about 5 times longer during the ABLE 3A program than those used during the ABLE 3B program. PAN and PPN measurements were taken using 1- to 2-min sampling times with individual samples taken every 6-to 10-min. NO_x and NO_y signals were recorded for 30-s signal integration times with individual measurements reported using longer integration times ranging from 1.5 to 3 min. Selection of the data set used here for investigating closure within the reactive nitrogen budget (i.e., NO_y versus ΣNO_y(i)) took into account this disparity in temporal overlaps of various NO_y(i) and NO_y measurements in relation to the magnitude of ambient variability observed in individual NO_y(i) compounds during the period of comparison. Because the HNO_3 measurement had the longest sample integration time, we chose to evaluate the budget based upon examining the average values of PAN, PPN, NO_x, NO_y, and other chemical variables observed during the HNO_3 sample integration period.

To account for effects that might arise from poor temporal overlap of the data during periods with large ambient variability, our NO_y to ΣNO_y(i) budget comparison data subset was filtered at two levels. First, the data were filtered to include only those HNO_3 measurement periods when all other NO_y(i) compounds (PAN, PPN, and NO_x) and NO_y were also measured. This filter required a 65% temporal coverage by the NO_x and NO_y measurements and similar temporal coverage by PAN within the framework of the PAN instrument's lower measurement duty cycle (i.e., PAN measurements 20% maximum temporal overlap could yield 13% temporal coverage of the HNO_3 measurement interval). The second filter that was used involved the examination of the temporal behavior of NO_x, NO_y, and PAN during individual HNO_3 measurement periods. Cases in which significant changes occurred in either NO_y, NO_x, or PAN mixing ratios that were not accompanied by measurements of all three compounds were excluded from the filtered data set.

Figures 1-3 display three examples of poor temporal overlap among the various N_xO_y measurements during periods of ambient variability. In the first two cases, NO_y mixing ratios were observed to increase by twofold to threefold in the middle of an individual HNO_3 measurement period, with PAN measurements occurring either outside of (see Figure 1), or at the center of (see Figure 2) the time period over which NO_y mixing ratios peaked. Each figure also illustrates the fraction of HNO_3, NO_x, and PAN (+PPN) to NO_y for the individual HNO_3 measurement period depicted in the time series plots and for nearby HNO_3 measurement periods that were selected by our filter to be valid N_xO_y budget comparison data

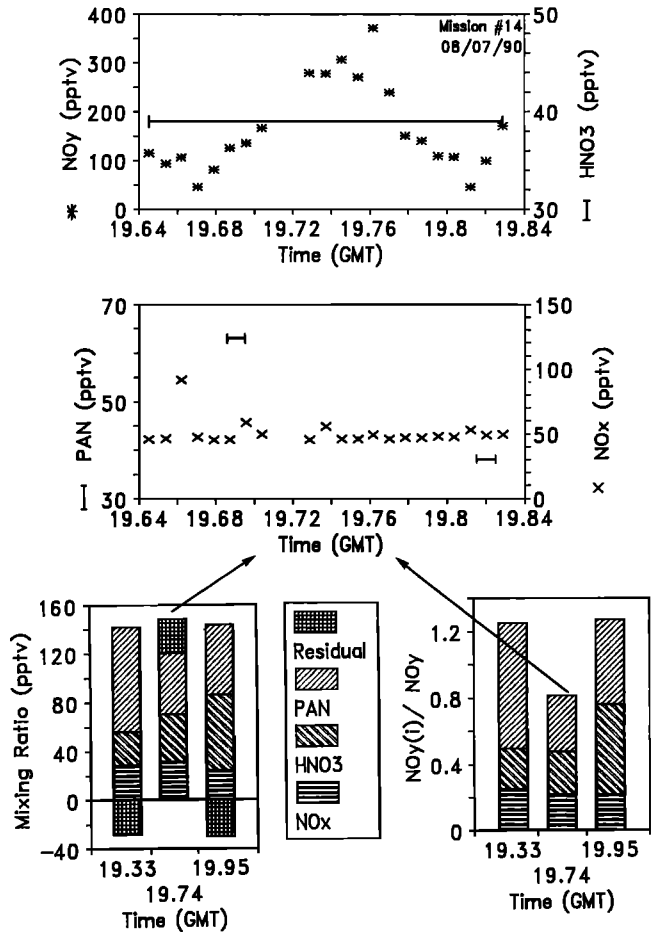

Fig. 1. Time series of different $NO_y(i)$ species and NO_y for Arctic Boundary Layer Expedition (ABLE) 3A mission 14, where mixing ratios (parts per trillion by volume) are represented by PAN (dash), HNO_3 (dash), NO_x (cross), and NO_y (asterisk), and the bar graphs for both the absolute mixing ratios and the fraction of NO_y are in the bottom left and right, respectively.

points. Figure 3 displays an example in which the HNO_3 measurement period coincided with a large increase in both NO_x and NO_y. In this case, PAN was measured only during the trailing edge of the event. All three of these cases and others like them were dropped from consideration due to poor temporal coverage during periods of ambient variability, as defined by a greater than 1.5-fold change in NO_y mixing ratios over a HNO_3 measurement period without concurrent measurements of PAN and NO_x.

There were 84, 134, and 144 HNO_3 measurements made over the Alaska, Hudson Bay lowland, and Labrador boreal forest study regions, respectively. The filtering, discussed above, produced a budget comparison data subset that retained 34, 69, and 89 HNO_3 measurement periods, or 40%, 51%, and 62% of the original database. The larger retention of data from the ABLE 3B database was primarily due to a combination of shorter HNO_3 sampling times and a 1- to 1.5-hour transit time between the base airports and the intensive study areas. These transits generally consisted of stair-step flight profiles that were optimized for the study of N_xO_y budgets in the free troposphere.

Table 1 gives a summary of the N_xO_y composition observed in the filtered data set for the Alaska, the Hudson Bay lowlands, and the northern Labrador/Quebec study regions. These data have been separated into measurements made in the middle free troposphere (from 3 km to 6.2 km) and those made in the planetary boundary layer (taken here as < 3 km). Inspection of Table 1 reveals that mean NO_x mixing ratios over both Canadian study regions were larger than those observed over Alaska by approximately 1.5-fold above 3 km and by 2-fold below 3 km. Over Canada the enhanced NO_x mixing ratios below 3 km may reflect the combination of warmer temperatures and the approximate threefold larger PAN mixing ratios. This increase in both the average NO_x and the PAN mixing ratios has been attributed to biomass burning [*Talbot et al.*,

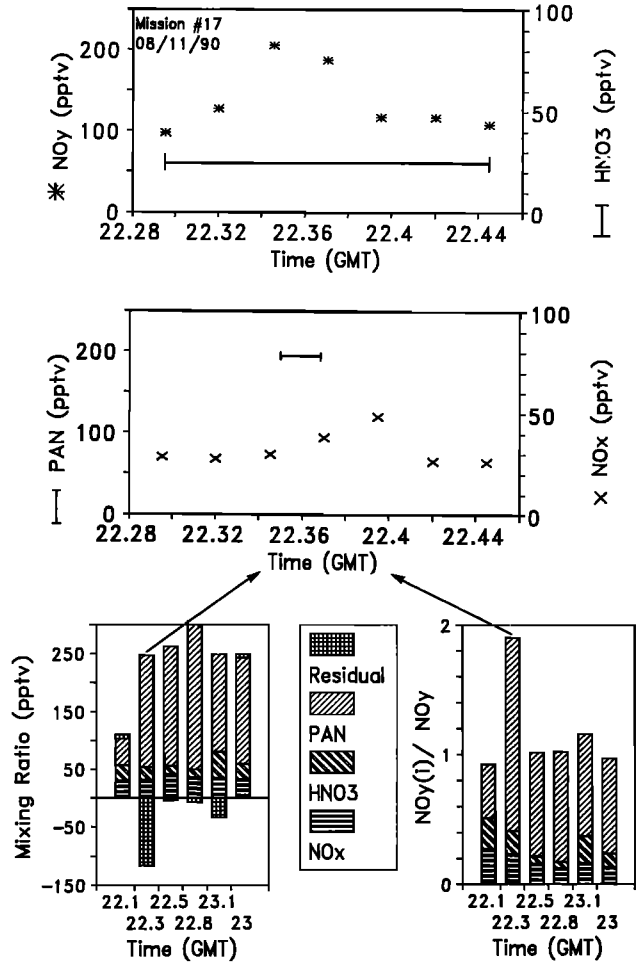

Fig. 2. Time series of different $NO_y(i)$ species and NO_y for Arctic Boundary Layer Expedition (ABLE) 3A mission 17, where mixing ratios (parts per trillion by volume) are represented by PAN (dash), HNO_3 (dash), NO_x (cross), and NO_y (asterisk), and the bar graphs for both the absolute mixing ratios and the fraction of NO_y are in the bottom left and right, respectively.

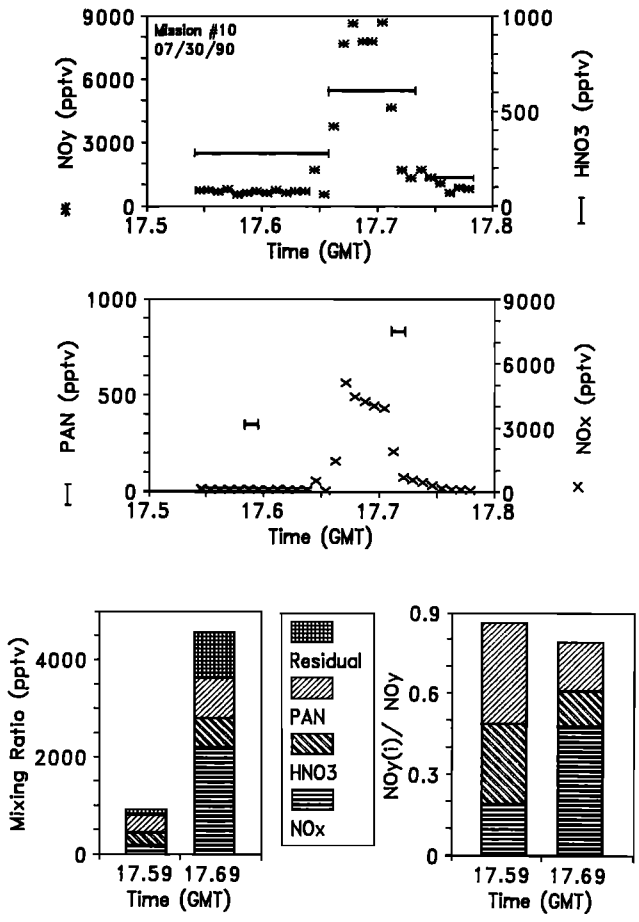

Fig. 3. Time series of different $NO_y(i)$ species and NO_y for Arctic Boundary Layer Expedition (ABLE) 3B mission 10, where mixing ratios (parts per trillion by volume) are represented by PAN (dash), HNO_3 (dash), NO_x (cross), and NO_y (asterisk), and the bar graphs for both the absolute mixing ratios and the fraction of NO_y are in the bottom left and right, respectively.

this issue]. Mean PAN mixing ratios above 3 km were nearly constant over all three study regions, even though median values were approximately 20% smaller over Alaska. Like its NO_x precursor (and PAN reservoir), below 3 km mean HNO_3 mixing ratios were also larger by approximately 1.5-fold over Canada. However, above 3 km, mean HNO_3 mixing ratios were approximately twofold smaller over Canada, even though median values were similar for all three locations. This difference between mean and median values may reflect a lower frequency of precipitation for the air masses encountered over Alaska [*Shipham et al.*, 1992; *Shipman et al.*, this issue]. Overall, the $\Sigma NO_y(i)$ above 3 km was relatively constant between all study regions, whereas below 3 km the values varied with the changes discussed above in PAN, NO_x, and HNO_3. In contrast, below 3 km, NO_y mixing ratios were approximately the same over Alaska and the Hudson Bay lowlands, whereas over northern Labrador/Quebec the values were approximately 35% smaller. Above 3 km, NO_y mixing ratios changed by approximately a factor of 2 between the Hudson Bay lowlands and the northern Labrador/Quebec study regions, with the average value over Alaska falling in between.

3.3. *Comparison of the Partitioning Observed in Nonurban Air*

The partitioning of compounds within the N_xO_y budget is summarized in Table 2. Also included are the partitionings observed in several other field programs that were recently summarized by *Ridley* [1991]. The comparison listed in Table 2 omits the contributions from $p\text{-}NO_3^-$ due to the uncertainties associated with its contribution to measured NO_y, or for that matter the "reactive" N_xO_y budget (see also discussions by *Atlas et al.* [1992]). PAN constitutes the largest fraction of NO_y in the Alaskan and Canadian middle free troposphere during the ABLE 3 study periods. The PAN fraction in this altitude range is similar to the middle free tropospheric values observed over the western continental United States during the CITE 2 field program even though the mean mixing ratio of PAN is approximately twofold smaller in the CITE 2 study. This smaller mixing ratio of PAN may reflect the warmer temperatures, which favor a faster thermal decomposition rate of PAN. This trend is maintained in the dramatically smaller PAN/NO_y fraction and mixing ratios observed at Mauna Loa, Hawaii (cf. PAN lifetimes given by *Singh et al.* [1990] and *Singh et al.* [1992b]).

As with other measurements in the remote troposphere, NO_x contributes only a small fraction to the NO_y budget observed over the North American high latitudes. The NO_x fraction of the NO_y budget (NO_x/NO_y) was smallest (~ 0.05) in the middle free troposphere over Alaska and the Hudson Bay lowlands. In these cases the median $NO_x/\Sigma NO_y(i)$ ratio (~0.12) is similar to values observed over northern Labrador/Quebec, the eastern Pacific, the western continental United States, and at Mauna Loa. In the northern Labrador/Quebec air masses that were characterized as having tropical origins, mixing ratios of NO_x were within the range of values that have been reported for midtropospheric air masses over the Pacific (compare recent review by *Ridley* [1991] and Table 2 to Table 3). In these modified tropical air masses, mixing ratios of NO_y also fall within the range of values for downslope (free tropospheric) flow conditions at Mauna Loa, even though PAN mixing ratios are considerably larger than those observed at Mauna Loa.

HNO_3 also represents a small fraction of the NO_y budget (~0.12) in the high northern latitude middle free troposphere. In the 3- to 6.2-km altitude range over the Alaska and Hudson Bay lowland regions, the HNO_3 fraction of NO_y is small in comparison to nonurban values from other studies, with the exception of those at Niwot Ridge, Colorado. These trends may be due to the variable scavenging and wash-out rates affecting different air masses and suggest HNO_3 is a poor choice to use for identifying trends in many cases.

TABLE 1. Summary of N_xO_y Compounds Observed Over Alaska and Canada

	NO	NO_2	NO_x	PPN	PAN	HNO_3	p-NO_3^-	$\Sigma NO_y(i)$	NO_y	Res.	Temp.	D. P.	CO	O_3	PAN/NO_x	HNO_3/NO_x
Alaska, < 3km (N=23)																
Mean	7.4	15	23	NR	35	73	28	125	349	223	9.6	4.1	103	37	1.4	3.2
Median	6.6	14	19	NR	17	50	16	90	284	194	11	5.8	103	32	0.94	2.7
Standard Deviation	4.3	6.3	9.8	NR	43	62	24	104	186	120	5.5	5.2	15	11	1.3	1.7
Minimum	3.6	7.5	15	NR	7.5	20	7	47	157	30	-2.6	-8.3	86	21	0.37	0.98
Maximum	22	33	55	NR	209	335	103	572	1010	437	19	11	141	70	5.0	6.3
Alaska, > 3km (N=11)																
Mean	11	19	31	9	278	100	26	397	669	272	-11	-23	113	78	9.2	3.0
Median	11	19	31	9	234	45	17	378	639	305	-12	-24	112	78	8.8	2.5
Standard Deviation	3.5	4.4	6.6	1.7	89	101	23	175	185	74	4.4	3.9	15	7.2	2.5	2.7
Minimum	5.5	11	18	7	162	20	12	207	434	126	-18	-32	96	66	5.7	0.77
Maximum	18	26	39	12	458	375	96	840	1180	347	-4.8	-18	138	90	13	9.8
Hudson Bay Lowlands, < 3km (N=43)																
Mean	10	38	48	0.2	95	120	11	252	340	89	16	7.7	127	37	1.8	2.3
Median	8.5	32	41	0	50	81	7.8	190	251	102	16	7.3	132	33	1.3	1.9
Standard Deviation	4	21	23	0.6	89	94	10	180	195	65	4.8	3.4	20	10	1.4	1.3
Minimum	5	15	21	0	13	13	4	62	112	-38	5.8	2.1	94	25	0.39	0.51
Maximum	22	95	103	3	318	338	40	670	749	268	28	14	160	73	6.5	5.0
Hudson Bay Lowlands, > 3km (N=26)																
Mean	13	35	48	0.7	302	67	30	399	841	442	-9.4	-21	109	64	6.9	1.7
Median	11	30	43	0	317	51	8.2	386	735	345	-11	-21	99	61	6.3	1.2
Standard Deviation	6.5	15	21	1.1	148	49	54	144	400	358	5.8	12	22	13	3.6	1.3
Minimum	4.7	16	21	0	41	10	4	191	383	124	-18	-42	88	45	1.1	0.09
Maximum	28	88	116	5	756	212	180	849	2000	1540	3.0	3	176	93	13	4.7
Northern Labrador/Quebec, < 3km (N=52)																
Mean	8	32	40	0.2	87	116	9.6	233	253	20	11	3.3	102	32	2.4	2.6
Median	6.9	25	33	0	61	69	7.1	191	202	-3.5	10	2.5	96	28	1.9	2.3
Standard Deviation	4	24	28	0.9	65	106	7.6	164	190	88	6.7	7.3	20	12	1.7	1.7
Minimum	3.6	12	18	0	14	11	4	52	60	-177	-1.7	-22	82	18	0.38	0.51
Maximum	29	142	158	4	280	437	40	807	920	201	24	17	166	59	8.5	7.0
Northern Labrador/Quebec, > 3km (N=37)																
Mean	9.8	33	43	0.6	295	50	6.5	371	459	89	-7.9	-18	100	55	7.4	1.2
Median	8.4	30	45	0	298	45	4	394	338	-14	-6.4	-20	100	57	6.7	0.84
Standard Deviation	4.5	12	14	1.5	106	36	4.2	124	487	444	5.9	9	18	8.6	3.1	0.89
Minimum	3.1	15	20	0	49	10	3.7	94	113	-175	-21	-41	64	35	1.6	0.21
Maximum	18	72	75	6	518	136	19	621	3250	2680	2.0	-0.3	142	79	15	4.7

$\Sigma NO_y(i)$ does not include p-NO_3^-. Mean and median $\Sigma NO_y(i)$ residual (Res.), PAN/NO_x, and HNO_3/NO_x are taken from individual data points (e.g. not mean of means). Mixing Ratios of NO, NO_X, PAN, HNO_3, p-NO_3^-, $\Sigma NO_y(i)$, NO_y, and residual (Res. = NO_y-$\Sigma NO_y(i)$) are in parts per trillion by volume. Mixing Ratios of CO and O_3 are in parts per billion per volume, temperature (°C), D.P. (Dew Point °C).

TABLE 2. Partitioning and Balance of N_xO_y

	NO_x/NO_y	HNO_3/NO_y	PAN/NO_y	$\Sigma NO_y(i)/NO_y$	NO_y	CO/NO_y	O_3/NO_y	C_3H_8/C_2H_6
				Alaska, 1988				
< 3 km	0.07	0.18	0.07	0.32	275	0.37	0.12	0.1
3 - 6.2 km	0.045	0.08	0.39	0.52	650	0.17	0.12	0.12
				Hudson Bay Lowlands, 1990				
< 3 km	0.15	0.34	0.19	0.73	250	0.24	0.12	0.1
3 - 6.2 km	0.055	0.065	0.4	0.51	750	0.14	0.085	0.11
				Northern Labrador/Quebec, 1990				
< 3 km	0.19	0.37	0.39	1.03	200	0.73	0.16	0.11
3 - 6.2 km	0.12	0.095	0.79	1.01	350	0.27	0.16	0.11
				Modified Tropical Air Over Northern Labrador/Quebec, 1990				
3 - 6.2 km	0.16	0.09	0.64	0.83	225	0.37	0.21	0.035
				*Eastern Pacific, Summer 1986 * CITE 2*				
4.6 - 5 km	0.09	0.32F-0.49D	0.33	0.78F-0.9D	425			
				*Western Continental United States, Summer 1986 * CITE 2*				
4.6-6.1 km	0.14	0.32F-0.16D	0.42	0.9F-0.7D	375			
				Niwot Ridge, Summer 1984 †				
3 km	0.25	0.095	0.17	0.52	2100			
				*Niwot Ridge, Summer 1987 **				
3 km	0.32	0.10	0.24	0.73	1600			
				MLOPEX Downslope, Spring 1988 ‡				
3.4 km	0.14	0.43	0.047	0.79	253			

The values in the table are median ratios not ratios of medians unless otherwise noted. Ratios of NO_x, HNO_3, PAN, and $\Sigma NO_y(i)$ to NO_y and C_3H_8/C_2H_6 are pptv/pptv, whereas CO and O_3 to NO_y are ppbv/pptv.

*From *Ridley* [1991], where the range of values given in Chemical Instrumentation Test and Evaluation 2 denote the range of HNO_3 mixing ratios using two different techniques and where (F) and (D) denote filter pack or denuder HNO_3 measurements.

†From *Fahey et al.* [1986], where the values are ratios of means extrapolated from their Figure 12 for daytime measurements.

‡From *Atlas et al.* [1992], where $\Sigma NO_y(i)/NO_y$ includes contributions from p-NO_3^- (~0.06) and alkyl nitrates (~0.01).

In the middle free troposphere over Alaska and Hudson Bay lowlands, only about 55% of the measured NO_y was accounted for by the measured $NO_y(i)$ species, which translates to a budget deficit ranging from approximately 300 to 400 pptv. At lower altitudes the $\Sigma NO_y(i)$ accounted for approximately 40 to 70% of the measured NO_y, resulting in NO_y budget deficits ranging from approximately 200 to 100 pptv, respectively. *Ridley* [1991] has presented arguments against *insitu* production increasing the absolute abundance of unaccounted for $NO_y(i)$ compounds during air mass aging. The relative abundance of chemically stable unaccounted for $NO_y(i)$ compound or compounds could, however, be increased during air mass aging as the active NO_x pool is converted via OH oxidation (or N_2O_5 hydrolysis) to HNO_3, which can be lost via scavenging processes. The magnitude of the deficit over Alaska and the Hudson Bay lowlands is larger, by about twofold to fourfold, than lower-latitude free tropospheric observations. The magnitude of the deficit in the NO_y budget is, however, at the lower end of the 0.2 to 1.5 ppbv range of mixing ratios that would occur from the 6 to 25% NO_y deficits that have been observed in rural areas of the continental United States [e.g., *Parrish et al.*, 1993]. The influx and dilution of these quantities of unaccounted for NO_y compounds could contribute to a portion of the NO_y budget deficit observed over some high-latitude regions [*Sandholm et al.*, 1992; *Wofsy et al.*, 1992]. For industrial pollutants to represent the compounds that form the deficits observed at all altitudes, they would, however, need to be more thermally stable than PAN. As previously discussed, there were some indications that the decomposition of PAN could not fully account for the NO_x mixing ratios observed in the 4- to 6-km altitude range over Alaska [*Jacob et al.*, 1992]. If true, this would suggest a portion of the NO_y deficit may act as a reservoir for the production of active odd nitrogen (NO_x). In the following sections we will attempt to address these hypotheses by investigating the factors that might be influencing the observed degree of closure within the high-latitude N_xO_y budget.

3.4. *Degree of Closure Within N_xO_y Budget*

In our examination of the degree of closure between NO_y and the $\Sigma NO_y(i)$ within the filtered N_xO_y budget comparison data subset, we feel it is necessary to take into account the measurement uncertainty of the individual $NO_y(i)$ species relative to NO_y. In general, each technique's claimed precision and accuracy has been generally demonstrated, based on the average observed mixing ratios using multiple techniques for the measurement of NO, NO_2, PAN, and HNO_3 (see earlier discussions in section 2). Based on the average level of agreement found in these intercomparison studies, the overall uncertainty at the 95% confidence limit for each measurement has been taken as ±25% for NO_x and ±30% for PAN (+ PPN), HNO_3, and NO_y. The relatively large uncertainty for NO_y is due to our inability to perform an *a priori* assessment of

TABLE 3. Summary of N_xO_y Compounds Observed in Air Classified As Having a Tropical Origin

Northern Labrador/Quebec, > 3km, and CO < 80 ppbv for "Tropical Air" (N=5)

	NO	NO_2	NO_x	PPN	PAN	HNO_3	p-NO_3^-	$\Sigma NO_y(i)$	NO_y	Res.	Temp.	CO	O_3	PAN/NO_x	HNO_3/NO_x
Mean	7.5	27	35	0	118	24	4	170	199	30	-7.4	73	42	3.4	0.75
Median	6.4	25	34	0	134	20	4	184	214	39	-4	71	43	3.0	0.59
Standard Deviation	3.8	4	6.7	0	44	12	0	50	46	47	4.6	6.0	4.9	1.2	0.40
Minimum	3.2	22	28	0	49	10	4	94	113	-24	-13	64	35	1.6	0.21
Maximum	14	33	47	0	169	46	4	238	243	98	-3.3	79	48	5.0	1.4

potential NO_y sampling problems, as many different compounds with different chemical properties are potentially involved (see discussion later in section 3.5).

Figures 4 and 5 display the degree of balance in the N_xO_y budget based on calculating the residual = NO_y - $\Sigma NO_y(i)$ (Figure 4) and the relative degree of balance (i.e., residual/NO_y, Figure 5) for the entire filtered N_xO_y budget data subset, where the $\Sigma NO_y(i)$ consists of NO_x, PAN (+PPN), and HNO_3. Measurements of CH_3ONO_2 were also reported for the Alaska studies. These CH_3ONO_2 measurements have been excluded from this analysis because the values were usually small in comparison to those of PPN and nearly negligible in comparison to those of PAN. In addition, the residual was calculated assuming an NO_y conversion efficiency of 0.95 for both PAN (+PPN) and HNO_3 based on the convertor efficiency characterizations results of *Fahey et al.* [1985]. These data have been segregated into three categories based on whether the absolute magnitude of the residual fell: (1) within one standard deviation of its estimated uncertainty (i.e., |residual| < 1σ, Figures 4*a* and 5*a*); (2) between one and two standard deviations of its estimated uncertainty (i.e., 1σ < |residual| < 2σ, Figures 4*b* and 5*b*); or (3) greater than two standard deviations of its estimated uncertainty (i.e., |residual| > 2σ, Figures 4*c* and 5*c*). This assessment was based on taking the overall uncertainty as the square root of the sum of the variances estimated above for NO_x, PAN, PPN, HNO_3, and NO_y (i.e., assuming that the variances are uncorrelated and random and the variance equals the square of the estimated measurement uncertainties).

Little altitude dependence is exhibited in either the absolute or the relative values of the residuals for the data having |residuals| < 1σ (see Figures 4a and 5a). In addition, these data are nearly evenly distributed about zero and are within the range ±100 pptv and ±0.2, respectively. The portion of the data having |residuals| between 1σ and 2σ (see figures 4b and 5b) is also distributed about zero, but with a larger number of points having positive residuals. In this category (i.e., 1σ < |residuals| < 2σ) the northern Labrador/Quebec data have fractional values that are more evenly distributed about zero than data from the Hudson Bay lowlands or Alaska. This tendency is especially pronounced for the portion of the data having |residuals| > 2σ. In the latter case, the number of points with negative residuals is not outside the range expected at the 95% confidence limit and tends to support the magnitudes of our overall uncertainty estimates. Based on these uncertainty constraints, we have adopted the following definitions for describing the NO_y to $\Sigma NO_y(i)$ budget, where (1) out-of-balance characterizes those data with positive valued residuals > 2σ and (2) in-balance characterizes those data with |residuals| < 2σ.

The abundance of $NO_y(i)$ and fractional abundance ($NO_y(i)/NO_y$) are given in Figures 6-8 for the three study regions. The data in these figures have been sorted by the fractional magnitude of the residuals. In addition to the $\Sigma NO_y(i)$ and NO_y data presented in Figures 6-8,

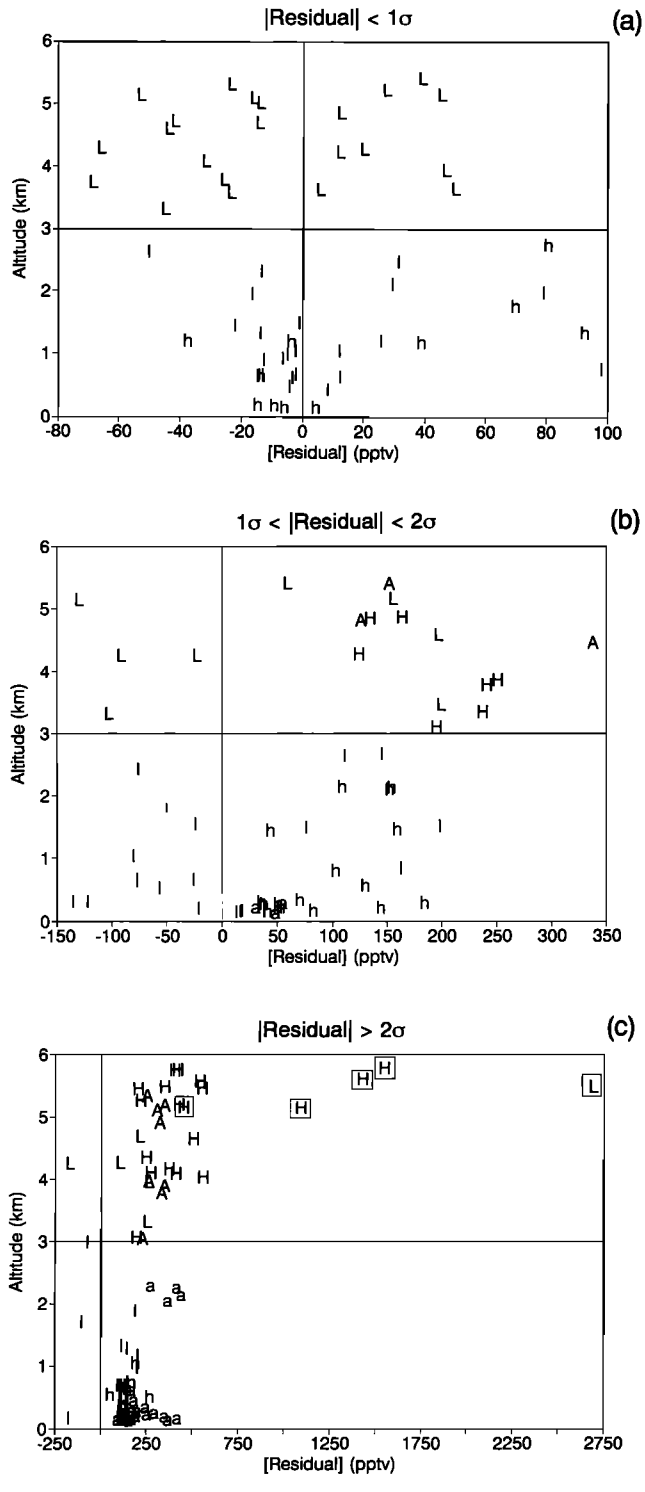

Fig. 4. Altitudinal dependence of the residual (residual = NO_y - $\Sigma NO_y(i)$) separated into one of three classifications: (*a*) |residual| is less than one standard deviation of the measurement uncertainties; (*b*) |residual| falls between one and two standard deviations of the measurement uncertainties; and (*c*) |residual| is greater than two standard deviations of the measurement uncertainties. A/a denote data from Alaska during ABLE 3A, L/l denote data from northern Labrador and Quebec during ABLE 3B, and H/h denote data from the Hudson Bay lowlands during ABLE 3B, where the uppercase letters indicate data taken between 3 and 6.2 km and lowercase letters indicate data taken at < 3 km.

particulate-nitrate ($p\text{-}NO_3^-$) mixing ratios are given when available, but they were not used in the calculation of residual values. Inspection of Figures 6-8 reveals that in general, even if it were sampled efficiently by the NO_y instrument, $p\text{-}NO_3^-$ should have contributed negligibly to the NO_y budget.

Below 3 km the NO_y to $\Sigma NO_y(i)$ budget for the Alaska data is clearly out-of-balance, having on average only about 35% of the NO_y accounted for by the $\Sigma NO_y(i)$. Above 3 km the data are also predominantly out-of-balance but with a larger fraction (~55%) of the NO_y accounted for by the $\Sigma NO_y(i)$. Above 3 km the Hudson Bay lowland data are also more out-of-balance. However, below 3 km the Hudson Bay lowland data are more evenly distributed with respect to overall estimates of the residuals' uncertainty. For this case, NO_y mixing ratios range from approximately 100 to 750 pptv, with a noticeable decrease in average values between the in- and out-of-balance categories (~ 400 pptv versus ~ 200 pptv, respectively). In contrast, over the northern Labrador/ Quebec study region the data from both altitude ranges (i.e., > 3 km and < 3 km cases) are predominantly in-balance with the $\Sigma NO_y(i)/NO_y$ ratio having a mean value near unity.

For comparison, a statistical summary of several of the in- and out-of-balance cases discussed above is given in Table 4. Below 3 km the out-of-balance Hudson Bay lowland data have mean mixing ratios that are approximately fourfold smaller for PAN and HNO_3 and approximately twofold smaller for NO_x and NO_y compared to the corresponding in-balance data. In this out-of-balance case the mean mixing ratios of the $NO_y(i)$ compounds and NO_y are closer to those observed in the lower-altitude Alaska data, which are predominantly out-of-balance (if the smaller mixing ratios of HNO_3 observed in the Hudson Bay lowland case were due to increased wet deposition). The in-balance northern Labrador/ Quebec data have nearly identical median mixing ratios of NO_x both above and below 3 km even though, as might be expected, PAN mixing ratios increased by approximately threefold in the higher-altitude regime. This increase in PAN mixing ratios more than offsets, by about twofold, the decrease in median HNO_3 mixing ratios allowing PAN to be the key species controlling the NO_y budget within this altitude range over northern Labrador/Quebec.

The larger fraction of in-balance data over northern Labrador/Quebec data may be due to a combination of factors. The dominant source of enhanced N_xO_y mixing ratios into the middle to lower (i.e., < 6 km) troposphere over the northern Labrador/Quebec region has been attributed to relatively fresh biomass burning emissions [*Talbot et al.*, this issue]. In addition, during the study period, there were several large influxes of what has been characterized as modified tropical air into the northern Quebec/Labrador region [see *Talbot et al.*, this issue; *Shipham et al.*, this issue]. In these air masses the mean mixing ratios of PAN, HNO_3, and NO_y are approximately twofold smaller than the corresponding mean values of the in-balance data set for this altitude range (cf. Tables 3 and 4). This suggests that the air masses over this region appear to have been influenced by both the influx of

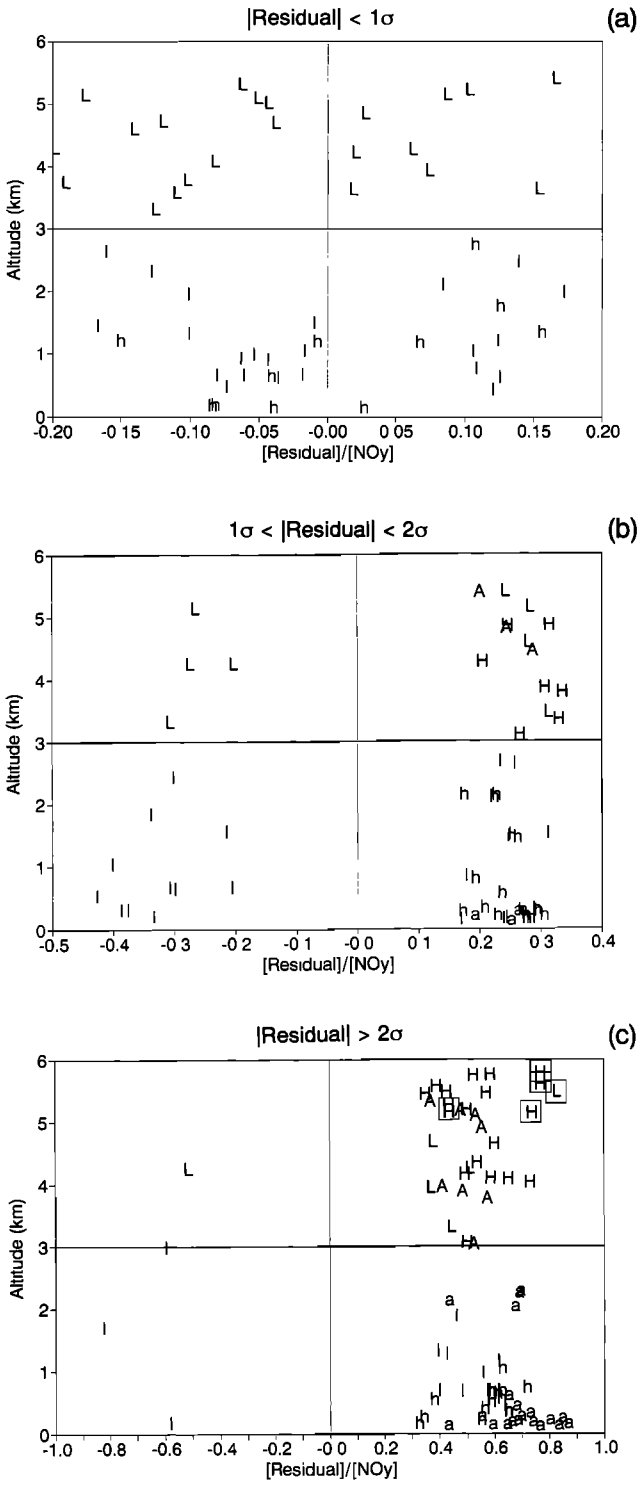

Fig. 5. Altitudinal dependence of the residual (NO_y - $\Sigma NO_y(i)$) relative to the measured NO_y mixing ratio (residual/NO_y) separated into one of the three classifications: (*a*) |residual| is less than one standard deviation of the estimated uncertainties; (*b*) |residual| falls between one and two standard deviations of the estimated uncertainties; and (*c*) |residual| is greater than two standard deviations of the estimated uncertainties. The data labels are described in Figure 4.

relatively well aged tropical air and the inputs of CO-rich and NO_y-poor emissions from smoldering combustion (see also discussions by *Talbot et al.* [this issue] and *Wofsy et al.* [this issue]. This may partially explain why the average mixing ratios of NO_y in both altitude ranges over northern Labrador/Quebec (i.e., ~ 250 pptv for < 3 km and ~ 460 pptv for > 3 km) were smaller than values observed over either Alaska or the Hudson Bay lowlands.

3.5. *N_xO_y Budget Implications of Trends Between NO_y and Other Components*

Implications of the correlative trends between individual $NO_y(i)$ and other measured compounds to the sources and sinks of reactive nitrogen are discussed in more detail by *Sandholm et al.* [1992], *Singh et al.* [1992 *a*, *b*, this issue], *Wofsy et al.* [this issue], and *Talbot et al.* [this issue]. Therefore in this section we will focus on investigating trends related to the NO_y versus $\Sigma NO_y(i)$ budget issue. Figures 9*a* and 9*b* illustrate the average correlation between mixing ratios of the individually measured $NO_y(i)$ compounds (i.e., NO_x, PAN, and HNO_3) and NO_y for both the in- and the out-of-balance data. Based on the linear regressions, these data suggest that on average there is an approximately threefold larger co-variance of NO_x with respect to NO_y for the in-balance data subset relative to the out-of-balance data subset. The small subset of out-of-balance data represented by a square is an aggregate of measurements made in plumes that had been cloud pumped to the aircraft's altitude (4 to 6 km; see also Figures 4 and 5). These plumes are believed to have originated from nearby biomass burning in the region. These data were not included in any of the calculated regressions for the out-of-balance data and, in general, the plume data will be discussed separately.

In contrast to the change in covariance implied from the NO_x versus NO_y regressions, the regression slopes for PAN versus NO_y imply that on average there is little change in the covariance relationship between the in- and the out-of-balance data. This might suggest that on average the out-of-balance data may represent more aged air parcels that had experienced a larger loss of NO_x (e.g., via OH + NO_x → HNO_3) relative to PAN. The lack of an enhanced HNO_3 to NO_y relationship or for that matter the lack of any strongly perceivable relationship in the out-of-balance data appears to contradict this hypothesis. However, as indicated by the small HNO_3 mixing ratios in the cloud-processed plume data, HNO_3 solubility precludes it from being a good surrogate for inspecting covariance relationships and suggests the need to examine correlations with respect to other trace gases.

Significant correlations between mixing ratios of O_3 and NO_y have been reported in several other free tropospheric studies. These studies have yielded fairly consistent linear regression slopes that are on average near 0.1 ppbv O_3/pptv NO_y, for NO_y mixing ratios less than approximately 450 pptv [*Hübler et al.*, 1992]. Of their reported studies,

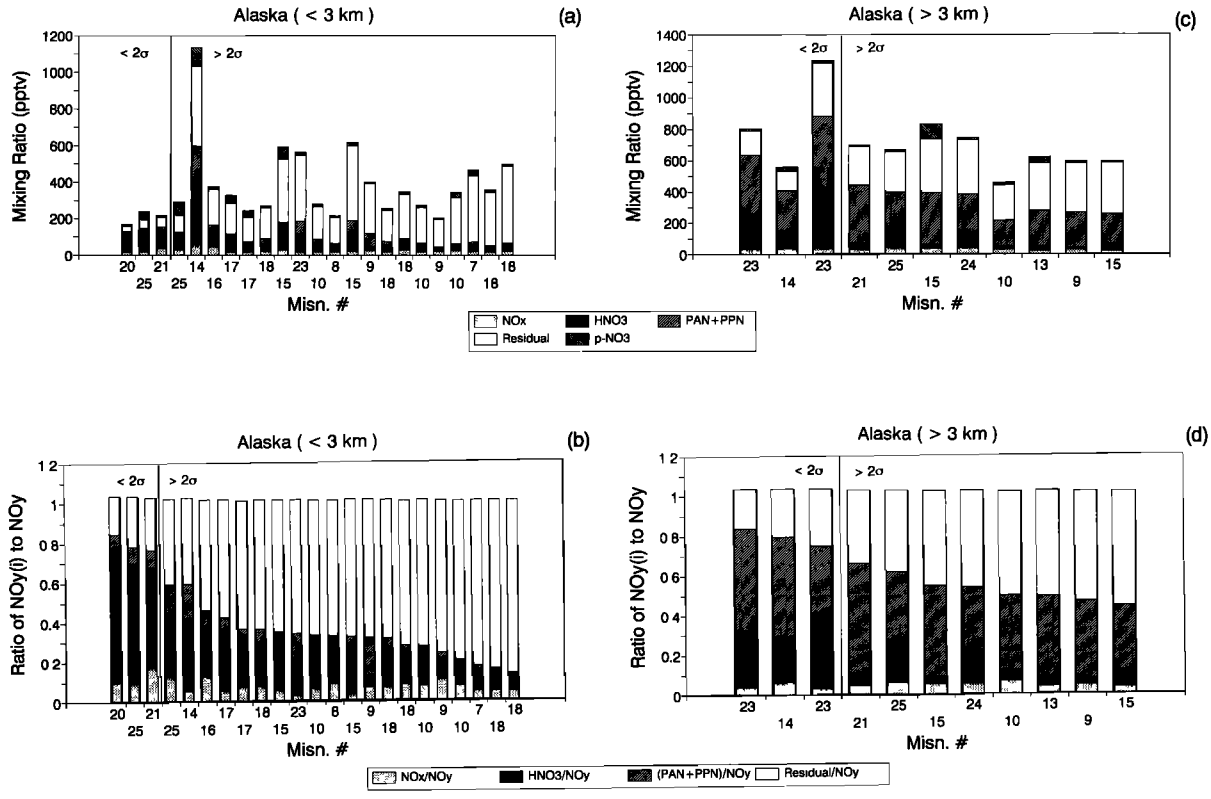

Fig. 6. ABLE 3A data from Alaska are represented in the stacked bar graphs, where (*a*) and (*b*) are for altitudes < 3 km and (*c*) and (*d*) are for altitudes between 3.0 to 6.2 km. Mixing ratios for the various NO_y(i) species and remaining residual values are illustrated in (*a*) and (*c*); stacking order from top to bottom: residual if positive; p-NO_3; PAN + PPN; HNO_3; NO_x; and residual if negative. The various NO_y(i) species and residual abundances relative to NO_y are illustrated in (*b*) and (*d*); stacking order from top to bottom: residual/NO_y if positive; (PAN + PPN)/NO_y; HNO_3/NO_y; NO_x/NO_y; and residual/NO_y if negative. There are no data less than one standard deviation of the residual's estimated uncertainties.

only the AASE 2 data appeared to maintain a linear O_3 to NO_y relationship at NO_y mixing ratios larger than approximately 450 pptv. For NO_y mixing ratios > 450 pptv, both the Mauna Loa Photochemistry Experiment (MLOPEX) and CITE 2 data exhibit a tendency toward less correlation between O_3 and NO_y, which is similar to the trend described by *Sandholm et al.* [1992] for composites of the ABLE 3A data taken over Alaska. The overall ABLE 3 N_xO_y budget subset of data exhibits a generally similar behavior (see Figure 10*a*). The correlation between mixing ratios of O_3 and NO_y appears to be a persistent feature in a significant portion of the northern hemisphere's free troposphere. In particular, the in- and out-of-balance data both exhibit similar degrees of correlation between O_3 and NO_y (cf. Figures 10*b* and 10*c*), even though the slope for the out-of-balance data is somewhat smaller (i.e., ~0.06 versus ~0.1). As might be expected, the slope of the O_3 versus ΣNO_y(i) regression for the NO_y < 450 pptv out-of-balance data is larger than the values obtained from the various O_3 versus NO_y regressions (i.e., 0.13 versus approximately 0.1 to 0.06; see Figure 11*a*; [*Hübler et al.*, 1992; *Sandholm et al.*, 1992]. Surprisingly, the slope of the O_3 versus residual for the out-of-balance data is also in the range of values discussed above (see Figure 11b). This slope, in combination with the slope from O_3 versus ΣNO_y(i), is of the correct magnitude to explain the smaller slope of the out-of-balance O_3 versus NO_y regressions. This correlation between O_3 and residual values suggests that on average the residuals have some degree of covariance with the factors influencing the troposphere's oxidative potential, as portrayed by O_3 mixing ratios, over these high-latitude regions.

Correlations have also been observed between mixing ratios of CO and NO_y in midlatitude urban and nonurban air masses [*Parrish et al.*, 1991]. These midlatitude data exhibited a nearly linear regression for mixing ratios of NO_y > 1 ppbv, with a linear CO versus NO_y regression slope near 20 (ppbv/ppbv). Below 1 ppbv, little correlation between mixing ratios of CO and NO_y was observed in their midlatitude data or in the midlatitude free tropospheric measurements made at Mauna Loa, where CO mixing ratios ranged from approximately 120 to 160

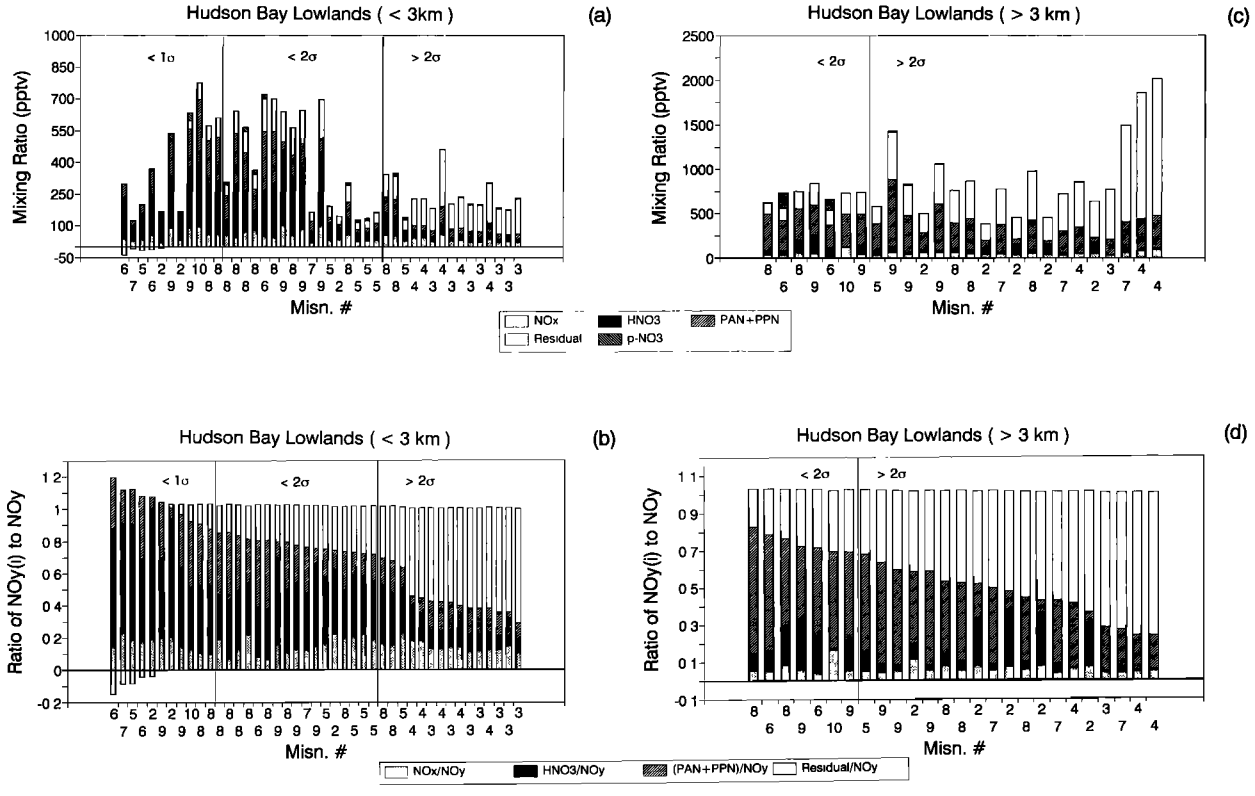

Fig. 7. ABLE 3B data from the Hudson Bay lowlands are represented as in Figure 6. There are no data less than one standard deviation of the residual's estimated uncertainties for altitudes greater than 3 km.

ppbv [*Hübler et al.*, 1992]. In contrast, the higher-latitude measurements of CO and NO_y presented here exhibit a linear correlation for NO_y mixing ratios < 1 ppbv and for CO mixing ratios generally below those found at Mauna Loa (see Figure 12a). The slope of this regression has a value that is approximately twofold larger than that obtained from the NO_y > 1 ppbv midlatitude data presented by *Parish et al.* [1991]. The larger CO versus NO_y slope may reflect the inputs of CO-rich/NO_y-poor emissions from high-latitude smoldering fires. Ratios of NO_y/CO have been observed to vary from approximately 0.0006 (±0.0003) for smoldering biomass burning [*Wofsy et al.*, 1992] to approximately 0.026 (± 0.005) for moderately aged plumes originating from the eastern U.S. [*Wofsy et al.*, this issue]. Based on laboratory experiments, biomass burning can have highly variable NO_y/CO emission ratios depending on whether flaming or smolderous combustion conditions are being supported (NO_y/CO ratios from about 1 to < 0.01, *Lobert et al.* [1990]). These variations in NO_y/CO ratios may help explain the loss in correlation going from the in-balance to out-of-balance subsets of data (r^2 = 0.92 versus r^2 = 0.70, cf. Figures 12*b* and 12*c*). In conjunction, the relatively small ratios of CO/NOy in the out-of-balance cloud-pumped plume data suggests these plumes may have originated from sources such as flaming biomass burning or industrial/urban pollution. These combined results suggest that all of these chemical signatures have been influenced by the emissions from a variety of sources.

To study further the possible causes for these trends, we have also investigated trends between values of NO_y, $\Sigma NO_y(i)$ and the residuals versus several surrogate time markers of the relative age of an air mass. We found little evidence of correlations with values of the parameter NO_y-NO_x, which has been successfully used as a "chemical-clock" that reflects the degree of oxidation in urban plumes when NO_x is the dominant $NO_y(i)$ species. Our data's lack of correlation with this parameter, NO_y-NO_x, is in agreement with the MLOPEX results presented by *Atlas et al.* [1992] and likely reflects their argument that in more aged air masses the NO_y to NO_x "chemical clock" has been continually reset by loss processes (e.g., wet removal) and recycling of odd nitrogen species.

Ratios of various carbon-containing compounds have also been used in numerous studies as surrogate "chemical clocks" that are not prone to resetting by such factors as rain/washout. However, they can be reset by the mixing in of fresh emissions that can have a variety of source emission factors and by the dilution of air parcels through the mixing in of background air having various ages (see S. McKeen and S. C. Liu, Hydrocarbon ratios and photochemical history of air masses, submitted to *Geophysical Research Letters*, 1993). Thus mixing and photochemical aging processes both contribute to

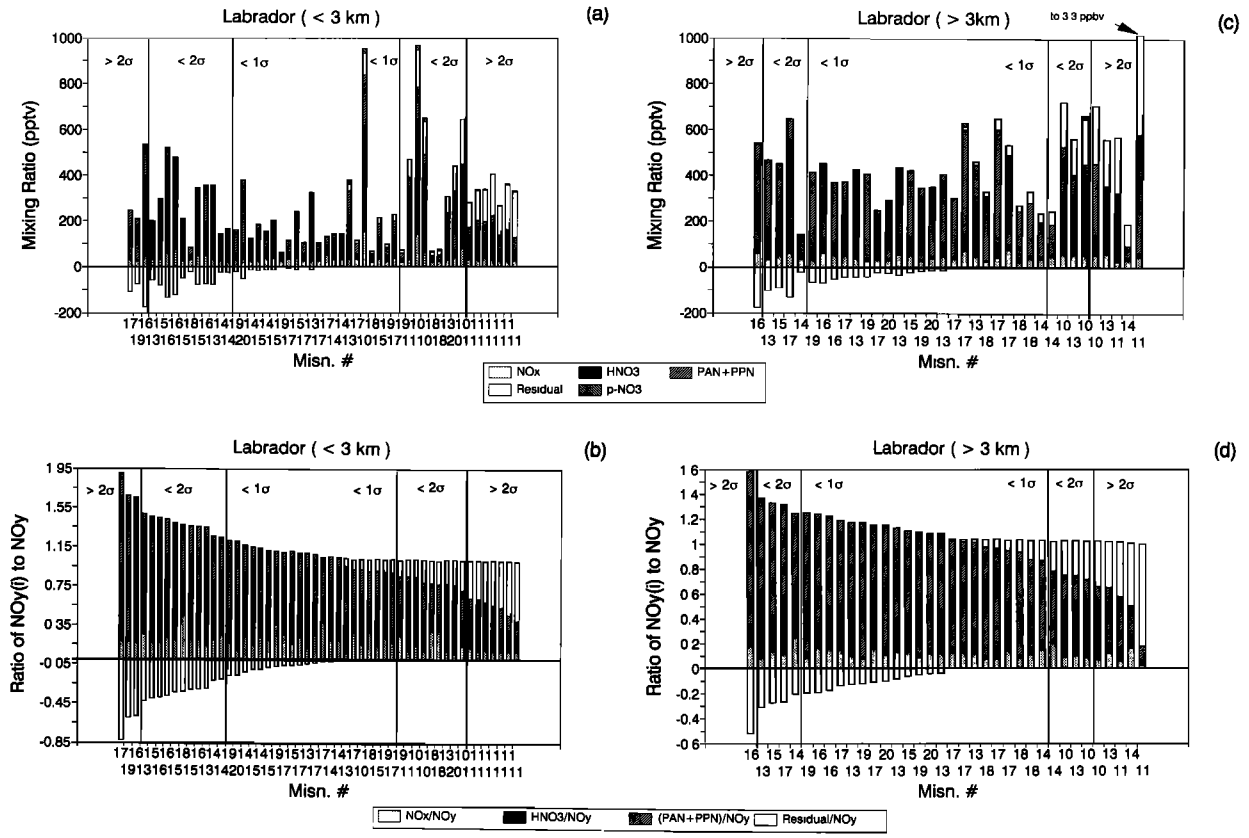

Fig. 8. ABLE 3B data from northern Labrador and Quebec are represented as in Figures 6 and 7.

establishing the ensemble average of an air mass's relative age. This precludes the unambiguous identification of sources and sinks based on any one "chemical clock's" estimate of an air mass's age and certainly precludes directly determining causation from any individual correlative trend. Thus, whereas it is tempting to argue that the on average correlation between O_3 and NO_y is suggestive of a common stratospheric source, it is perhaps more appropriate to suggest that this correlation merely reflects the common behavior of two species that are reasonably long-lived in the upper troposphere (as is CO) and that share similar loss rates due to photochemical and/or deposition processes as air parcels become distributed (and diluted) on a hemispheric scale. The small HNO_3 fraction of NO_y in these data sets also support this latter argument, unless an efficient mechanism can be identified that is capable of converting stratospherically derived HNO_3 back into more active forms of NO_y. Recent laboratory measurements indicate that NO_x can be generated from the surface catalyzed photolysis of H_2SO_4 and HNO_3 mixtures [D. Fahey, private communication]. These observations could suggest that a similar aerosol coupled mechanism might be responsible for reliberating the reactive nitrogen pool that has been thought to become irreversibly tied up as HNO_3. The implications of such possible mechanism to the distribution of NO_x over remote regions certainly warrant careful laboratory study. Another possible explanation is the residence time in the upper troposphere (> 6 km) is sufficiently long to allow OH oxidation and photolysis to slowly reactivate the stratospheric NO_x pool that is tied up in HNO_3.

Ratios of carbon containing compounds can still, however, provide some useful information about a particular air mass's combined photochemical history relative to other air masses. In particular, the ratios C_2H_2/CO and C_3H_8/C_2H_6 have been used to reflect the degree of combined mixing and photochemical processing that has occurred within an air mass (see discussion by *McKeen and Liu* [*ibid*]). During this atmospheric processing, the dominant tropospheric chemical loss process for all four compounds is their oxidative reactions with OH. The faster reaction rate coefficients [e.g., *DeMore et al.*, 1992] for C_2H_2 and C_3H_8 versus CO and C_2H_6 yield expectations that these two pair of ratios should have similar values that decrease as an isolated air mass photochemically ages. In our ABLE 3A investigations, NO_y was well correlated with ratios of C_2H_2/CO [*Sandholm et al.*, 1992]. This tendency also generally holds for both the in- and out-of-balance data (see Figures 13*a* and 13*b*). However, the out-of-balance cloud-pumped plume data do not follow the trend expected from either the in-balance or the nonplume out-of-balance data. These plumes did appear to be depleted of HNO_3 relative to NO_x or PAN, as discussed earlier. Somewhat surprisingly though, these plumes tend to follow the general trend exhibited between the ratios of C_2H_2/CO versus the

TABLE 4. Summary of in- and out-of-Balance Case Studies

	NO	NO_2	NO_x	PPN	PAN	HNO_3	p-NO_3^-	$\Sigma NO_y(i)$	NO_y	Res.	Temp.	NO_x/NO_y	PAN/NO_y	HNO_3/NO_y	$\Sigma NO_y(i)/NO_y$
Hudson Bay Lowlands, < 3km, in Balance (N=19)															
Mean	11	48	59	0.4	157	188	15	387	445	58	16	0.15	0.32	0.48	0.91
Median	9.7	46	58	0	171	194	12	429	532	70	16	0.15	0.37	0.41	0.87
Standard Deviation	4.3	20	22	0.9	99	69	13	155	201	62	5	0.05	0.12	0.17	0.12
Minimum	5.5	20	26	0	13	75	4	122	113	-37	5.8	0.07	0.08	0.26	0.76
Maximum	22	92	100	3	318	330	40	669	750	154	27	0.23	0.45	0.8	1.2
Hudson Bay Lowlands, < 3km, out of Balance (N=12)															
Mean	9	23	32	0	36	28	6	92	237	145	15	0.13	0.15	0.12	0.39
Median	7	17	25	0	31	22	4.6	77	205	125	13	0.13	0.15	0.11	0.38
Standard Deviation	4	8.4	11	0	17	11	1.7	33	74	43	4.2	0.02	0.03	0.03	0.4
Minimum	6	15	22	0	22	13	4	62	179	107	9.5	0.1	0.1	0.07	0.28
Maximum	20	40	60	0	86	52	7.8	190	458	268	22	0.18	0.19	0.18	0.45
Northern Labrador/Quebec, < 3km, in Balance (N=31)															
Mean	8	33	41	0.2	90	111	9	232	237	4.7	11	0.21	0.43	0.45	1.03
Median	6.8	24	31	0	60	62	7.1	156	138	-4.4	9	0.21	0.42	0.4	1.04
Standard Deviation	4.9	28	32	0.8	67	110	6.4	180	214	54	7	0.07	0.15	0.19	0.15
Minimum	3.6	12	18	0	25	14	4	60	60	-78	-1.7	0.08	0.17	0.15	0.77
Maximum	29	142	158	4	280	437	23	808	920	162	24	0.38	0.89	1.04	1.3
Northern Labrador/Quebec, > 3km, in Balance (N=26)															
Mean	8.5	32	40	0.4	300	50	6.1	374	352	-22	-8.6	0.12	0.85	0.15	1.1
Median	6.6	29	35	0	298	39	4	392	332	-24	-7.9	0.12	0.84	0.11	1.1
Standard Deviation	4	13	14	1.2	95	38	4	114	110	46	6	0.04	0.11	0.1	0.13
Minimum	3.1	15	20	0	86	10	3.7	137	113	-130	-21	0.07	0.64	0.03	0.83
Maximum	18	72	75	6	518	136	19	620	628	50	0.3	0.25	1.1	0.4	1.3

Mean and median $NO_y(i)$, Res., and ratios to NO_y are taken from individual data points (e.g. not mean of means).

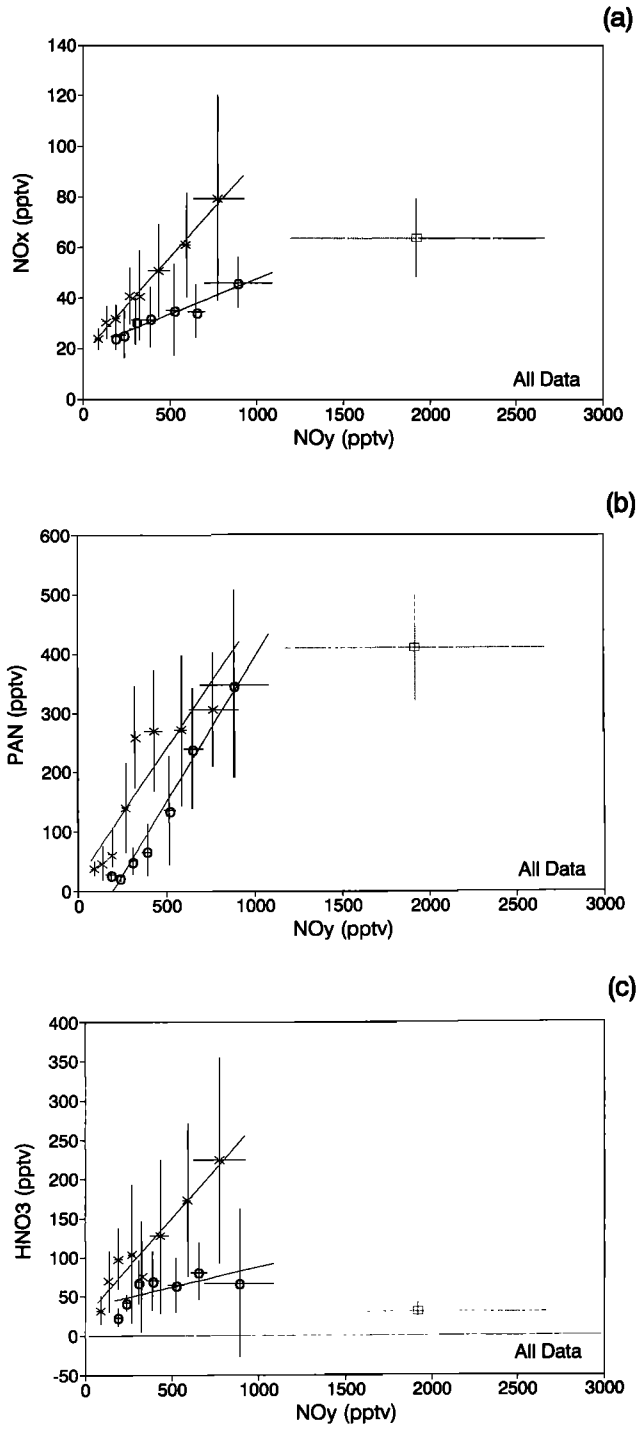

Fig. 9. Graphs of aggregated data for the NO_y(i) versus NO_y where the following represent data for in balance (cross), out of balance (circle), and cloud-pumped plumes (square) (see text); and where (*a*) NO_x versus NO_y (in balance slope = 0.077 ±0.003 with r^2 = 0.99 and out of balance slope = 0.028 ±0.004 with r^2 = 0.93); (*b*) PAN versus NO_y (in balance slope = 0.44 ±0.09 with r^2 =0.80 and out of balance slope 0.49 ±0.04 with r^2 = 0.97); with (*c*) HNO_3 versus NO_y (in balance slope = 0.25 ±0.03 with r^2 = 0.92 and out of balance slope = 0.051 ±0.027 with r^2 = 0.43). Horizontal and vertical bars represent plus and minus one standard deviation about the mean for each aggregate.

ΣNO_y(i) (see Figure 13*c*). This might suggest that the more reactive forms of NO_y (i.e., NO_x and PAN) may have been in sink with the average degree of atmospheric processing that had occurred in the middle/lower troposphere over these regions, whereas the substantial budget deficit for NO_y - ΣNO_y(i) may represent compounds that were significantly out of sink with the relative degree of atmospheric processing that is indicated by the ratios of C_2H_2/CO.

Ridley [1991] presented arguments that the abundance of a missing compounds implied from comparison of NO_y-ΣNO_y(i) are not enhanced during air mass aging. Our results agree with this argument. However, our results also indicate that the relative abundance of the implied missing compounds increases with the degree of atmospheric processing (see Figure 13*d*). This might be expected if the implied missing compounds are less susceptible than NO_x, PAN, and HNO_3 to atmospheric loss processes (e.g., oxidative attack in the case of NO_x, thermal decomposition in the case of PAN, and the final dry/wet deposition processes that remove the HNO_3 formed from NO_x and its reservoirs).

The in-balance mixing ratios of NO_y are also correlated on average with the degree of atmospheric processing established by the ratio C_3H_8/C_2H_6 (see Figure 14*a*). However, this trend tends to disappear in the out-of-balance data (cf. Figure 14*a* and 14*b*). This supports the argument that the various relative "chemical clocks" of the different air masses represented by these data were all perhaps on somewhat different cycles that reflect different degrees of mixing and photochemical ageing. We believe this is borne out by the loss in correlation between the ratios C_3H_8/C_2H_6 and C_2H_2/CO in going from the in-balance subset of data to the out-of-balance subset of data (cf. Figure 15*a* and 15*b*).

In general, our attempts at directly investigating the possible factors that influence the residuals have been complicated by (1) the apparent random resetting of selected surrogate "chemical clock" relationships, which appears especially pronounced in the out-of-balance data and (2) the generally random nature of the in-balance residual values that appears to be dominated by (1) the random uncertainties of the measurements and (2) the random uncertainties introduced by ambient variability in conjunction with the less than unity temporal overlap between the various NO_y(i) and the NO_y measurements, including perhaps sporadically enhanced p-NO_3^- events occurring within the long sample time of the aerosol measurements.

In addition to O_3 mixing ratios (see earlier discussion) the only other compounds that appear to correlate with the values of the out-of-balance residuals are the mixing ratios of PAN and perhaps NO_x and HNO_3 (see Figure 16*a*-16*c*). The correlation found between values of the residuals and the mixing ratios of O_3 and PAN would, again, suggest that the compounds comprising the measured NO_y budget deficit might have some degree of covariance with the factors influencing the oxidative potential of these air

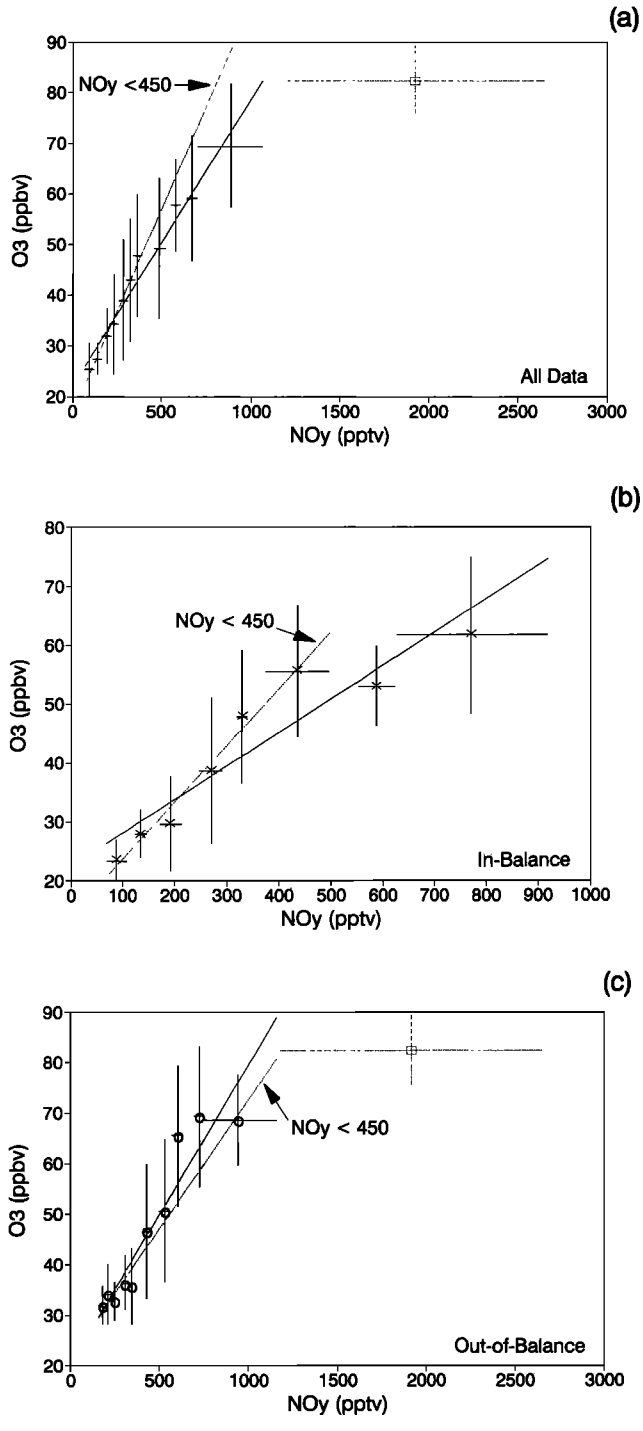

Fig. 10. Graphs of aggregated data for O_3 versus NO_y where the solid line is for all nonplume points and dashed line is for NO_y < 450 pptv: (*a*) all data (solid line slope = 0.057 ±0.003 with r^2 = 0.97, dashed line slope = 0.082 ±0.005 with r^2 = 0.98); (*b*) in balance (solid line slope = 0.057 ±0.009 with r^2 = 0.87, dashed line slope = 0.097 ±0.007 with r^2 = 0.98); and (*c*) out of balance (solid line slope = 0.059 ±0.007 with r^2 = 0.90, dashed line slope = 0.051 ±0.013 with r^2 = 0.80). Horizontal and vertical bars as in Figure 9.

masses. These trends might support *Jacob et al.'s* [1992] argument that in the summertime middle free troposphere over Alaska an additional reservoir-derived source of NO_x, besides that produced from the thermal decomposition of PAN, is necessary to account for the observed mixing ratios of NO_x. If the NO_y budget deficits represented compounds that are capable of generating NO_x, then they could also enhance the photochemical production rate of O_3 and possibly reinforce the observed O_3 to NO_y trends. However, it is doubtful that these missing compounds are simple alkyl nitrates based on the small fraction observed thus far for these compounds relative to NO_y or even PAN [*Atlas et al.*, 1992; *Buhr et al.*, 1990].

On average, the residual values are also negatively correlated with temperature (see Figure 16*d*). This is consistent with there being labile reactive odd nitrogen compounds other than PAN, such as HO_2NO_2, that are thermally stable in the cold upper troposphere [e.g., *Logan et al.*, 1981]. Even though thermally stable at high altitudes, HO_2NO_2 has not been predicted to be a major NO_y(i) species in the summertime high-latitude middle troposphere [*Singh et al.*, 1992; *Jacobs et al.*, 1992]. However, their estimates did not take into account the uncertainty associated with the equilibrium $HO_2 + NO_2 \rightleftharpoons HO_2NO_2$, which is large enough to result in an approximate fivefold uncertainty in calculated mixing ratios of HO_2NO_2 at 260 K [*DeMore et al.*, 1992]. At the upper limit of this range, steady state mixing ratios of HO_2NO_2 could exceed those of NO_2 by a factor of 10. At this limit, HO_2NO_2 would be a major component of the ΣNO_y(i) and might explain a portion of the NO_y budget deficit observed in the high-latitude middle troposphere. However, before we can attribute HO_2NO_2 to a missing portion of the NO_y budget, the formidable question as to whether or not HO_2NO_2 survives beyond the Teflon prefilter and can be quantitatively sampled by MC/IC technique must be answered.

An alternative explanation for these trends that we must also address is the possibility of one or more of the NO_y(i) or NO_y measurements is in error. Some types of errors in one or more of these measurements would still be consistent with the out-of-balance residual values being in some way correlated with factors influencing the oxidative potential of the air masses. In the case of NO_x it is unlikely that these measurements are in error by the very large factors (i.e., tenfold) that would be necessary to explain the budget deficit. This is based on the level of agreement, which has been shown in intercomparison programs, between this technique and the others (see discussion in section 2.1). In addition, potential NO_2 measurement interferences have a tendency to have positive values (e.g., $HO_2NO_2 \rightarrow NO_2$), which would argue that the NO_x values might already represent upper limits. In addition, the NO_x/NO_y and PAN instruments were intercalibrated using common NIST NO and NO_2 standards. This should have significantly reduced the potential for differences in primary standards being the cause of the NO_y budget deficit.

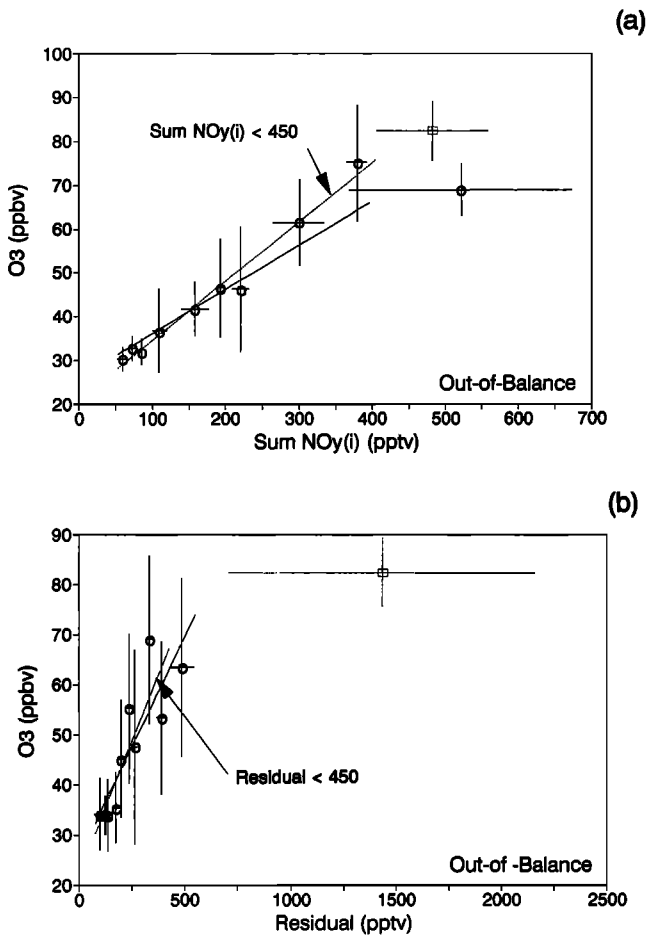

Fig. 11. Graphs of aggregated out of balance data where (*a*) O_3 versus $\Sigma NO_y(i)$ (slope for solid line = 0.10 ±0.01 with r^2 = 0.89, dashed line $\Sigma NO_y(i)$ < 450 pptv slope = 0.135 ±0.007 with r^2 = 0.98); (*b*) O_3 versus residual (slope for solid line = 0.087 ±0.019 with r^2 = 0.73 and dashed line residual < 450 pptv slope = 0.105 ±0.025 with r^2 = 0.71). Horizontal and vertical bars as in Figure 9.

In the case of PAN the necessary measurement errors would need to be of the order of factors of 1.5 to 3 (see Figure 16a). During the CITE 2 intercomparison, at times, 1.8-fold differences were observed between the data from the two airborne PAN instruments [*Gregory et al.*, 1990*c*]. A possible error of this magnitude in the PAN measurements would also be consistent with the behavior of the missing NO_x source suggested by *Jacob et al.* [1992]. However, it is noted that the PAN instrument used in the ABLE 3 studies was the one that on average reported larger (not smaller) PAN mixing ratios during the CITE 2 intercomparison. This would seemingly argue against the PAN measurements presented here being too small by factors of 2 to 3. In addition, we believe that the free tropospheric values of PAN that would be implied from the out-of-balance residual = PAN are unprecedentedly large.

An underestimate of HNO_3 could also be consistent with the observed trends. The 1988 MLOPEX results indicated an on average correlation between increasing HNO_3 mixing ratios and increasing values of the missing compounds that were implied by their NO_y budget analysis. The out-of-balance ABLE 3 data exhibit far less evidence of this tendency (cf. Figure 16*c* to Figure 6 in the work of *Atlas et al.* [1992]). These differences between the MLOPEX and

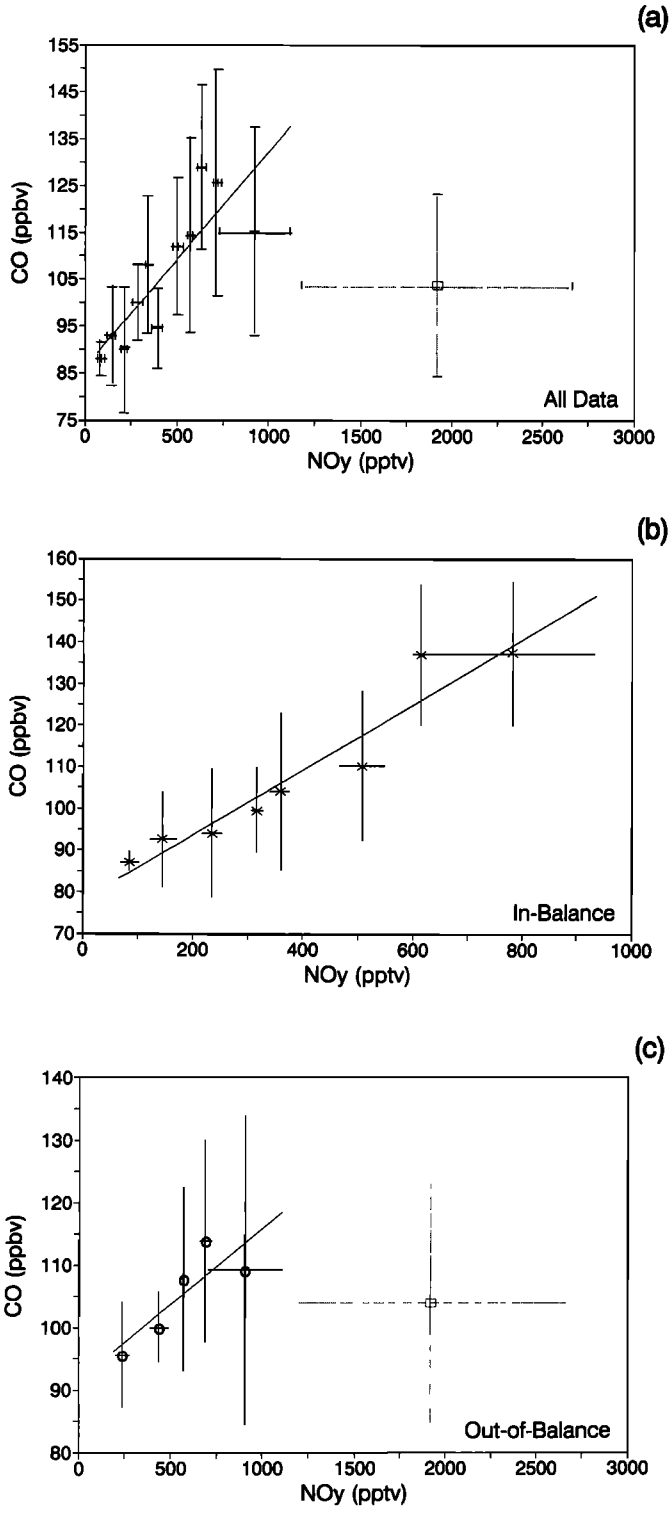

Fig. 12. Graphs of aggregated data for CO versus NO_y: (*a*) all data (slope = 0.040 ±0.016 with r^2 = 0.71); (*b*) In-Balance data (slope = 0.078 ±0.009 with r^2 = 0.92); and (*c*) out of balance data (slope = 0.024 ±0.009 with r^2 = 0.70). Horizontal and vertical bars as in Figure 9.

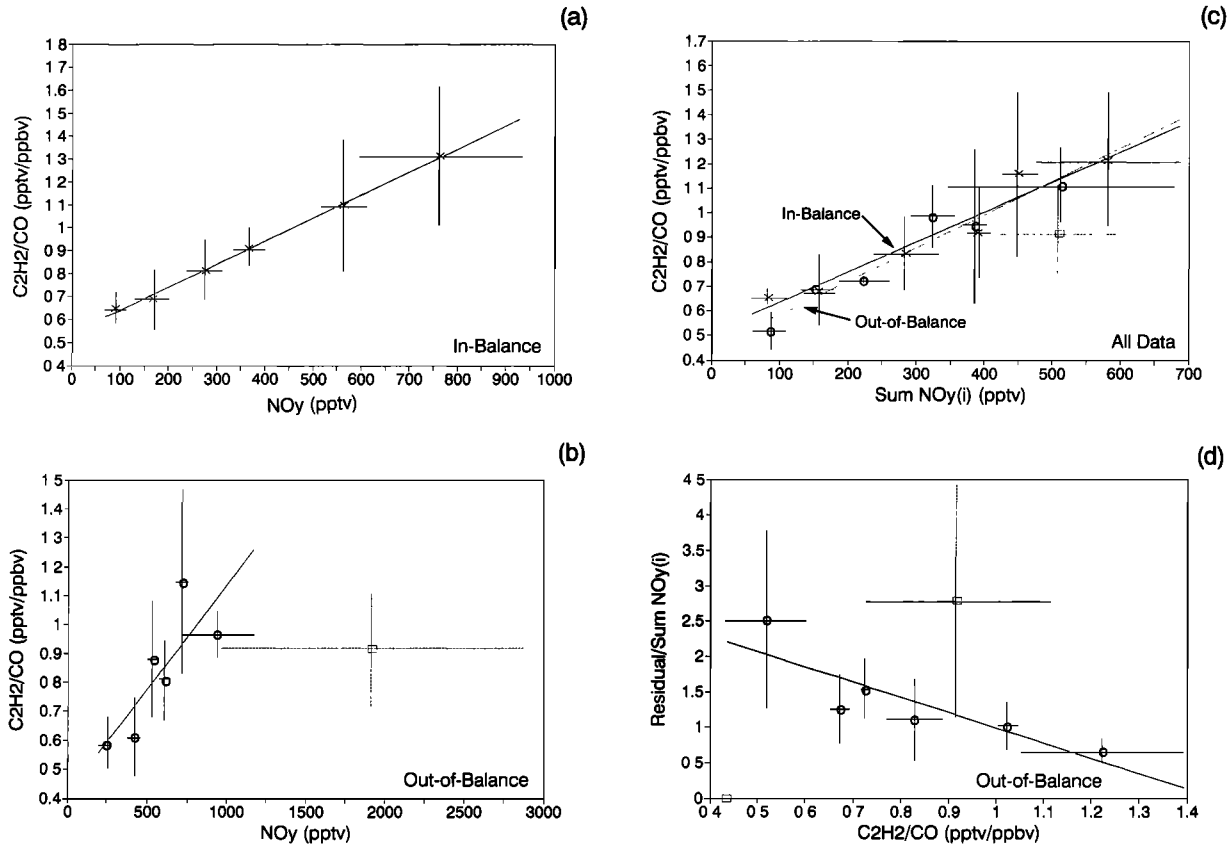

Fig. 13. Graphs of aggregrate data for (*a*) C_2H_2/CO versus NO_y using the In-Balance data (cross) (slope = 0.0010 ±0.00002 with r^2 = 0.998); (*b*) C_2H_2/CO versus NO_y using the out of balance data (circle) (slope = 0.00073 ±0.00037 with r^2 = 0.652); (*c*) C_2H_2/CO versus $\Sigma NO_y(i)$ (in balance data (cross) slope = 0.001 ±0.0002 with r^2 = 0.94, and out of balance data (circle) slope = 0.0012 ±0.00016 with r^2 = 0.94) without the cloud-pumped plumes (square) (see text); and (*d*) residual/$\Sigma NO_y(i)$ versus C_2H_2/CO using the out of balance data (slope = -2.15 ±0.64 with r^2 = 0.74). Horizontal and vertical bars as in Figure 9.

the ABLE 3 observations might simply be expected based on the differences in CO versus NO_y trends and differences in frequency of precipitation between the low to midlatitude and high-latitude sets of observations. Since there has been no airborne intercomparison evaluation of the MC/IC technique, it is difficult to evaluate if the magnitude of potentially unforseen measurement errors could significantly contribute to the observed trends. However, it is unlikely that a large random error exists as this would destroy the on average coherence displayed between PAN and O_3 versus NO_y for the out-of-balance data.

Similarly, in the case of NO_y we would not expect the out-of-balance correlative tendencies to exist between O_3 and NO_y or the PAN and the residual if the out-of-balance residuals were merely due to an offset type error (or artifact) in the NO_y measurements. Like the HNO_3 technique the NO_y technique has also not undergone airborne intercomparison evaluation, and several sampling/measurement uncertainties, which may be shared by one or more of the $NO_y(i)$ instruments, warrant discussion.

In principle, if a compound is merely converted to another detectable gas phase NO_y compound (e.g., $NO_{3(gas)}$ + surface → $NO_{2(gas)}$, or $HO_2NO_{2(gas)}$ + surface → $NO_{2(gas)}$), then the effective NO_y transmission efficiency of the inlet could remain high. However, if a gas phase NO_y compound reacts to form a new compound that can remain on the surface, or a compound that is more easily chemiadsorbed onto a surface (i.e., sticky compounds like HNO_3, e.g., $HO_2NO_{2(gas)}$ + hydrated surface → $HNO_{3(surface)}$), then the effective transmission efficiency of the inlet would decrease until all active sites are depleted, or a new temperature- and humidity- dependent equilibrium is established between the gas phase and the surface/substrate (in the case of permeable materials). As conditions change (e.g., temperature, pressure, humidity, and surface characteristics), a new set of equilibrium concentrations would also become established, which could either reduce the effective NO_y transmission of the system or artificially enhance the transmission. These effects could also apply to deposited NO_3^--containing aerosols and any aerosol reservoir of large polyfunctional organic odd-nitrogen containing compounds (compounds which would

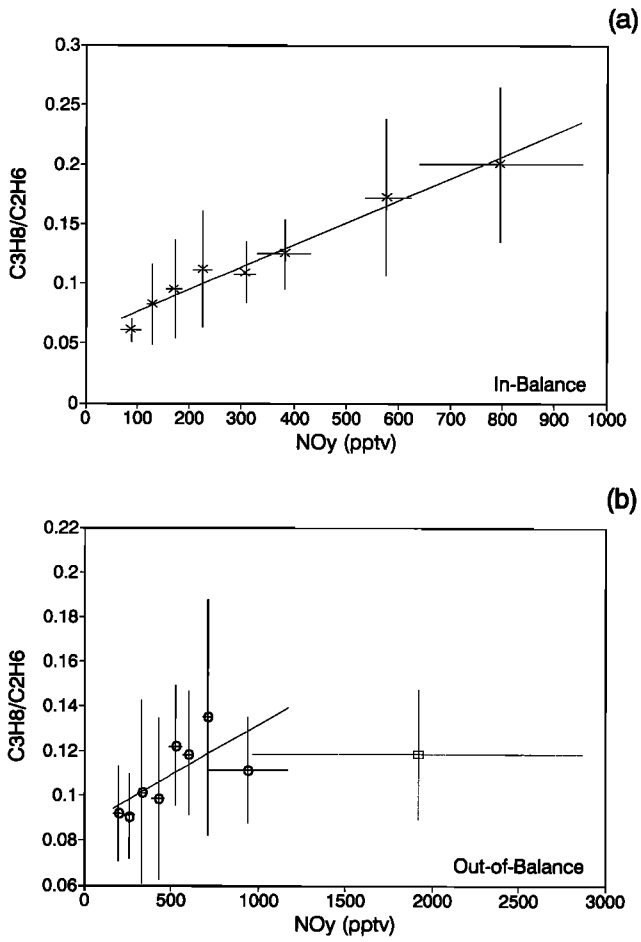

Fig. 14. Graphs of aggregated data for C_3H_8/C_2H_6 versus NO_y: (*a*) in balance (cross) (slope 0.00019 ±0.00001 with r^2 = 0.97) and (*b*) out of balance (circle) (slope = 0.000045 ±0.000018 with r^2 = 0.51). Horizontal and vertical bars as in Figure 9.

escape detection by the p-NO_3^- measurement technique). This combination of memory effects might generate both positive and negative artifacts that are difficult to quantify or simulate in the laboratory. In addition, the efficiency of transmitting NO_3^--containing or any R-NO_x-containing aerosols may vary as a function of pressure (i.e., altitude) and flow velocity depending on the sampling inlet geometry and sampling line characteristics. Similar arguments can also be made for the various NO_y(i) sampling systems. As noted in sections 2.1 and 2.3, some evidence of memory effects have been observed in both the NO_y and the HNO_3 measurement systems and may have affected some of the data presented here, especially when PFA Teflon tubing was used. All of the effects discussed above might result in somewhat random variations in instrument response. These variations could depend on the exact nature of not only the compounds constituting NO_y but also ambient conditions of temperature, pressure, and humidity and the condition of the inlet sampling line's surfaces. The HNO_3 and NO_y sampling inlets were, however, designed to have short sample residence times and small surfaces to volume ratios in order to minimize these potential problems. At this time though, we cannot rule out the possibility that the combined magnitude of these effects may be responsible for some of the random variations apparent in the in-balance data's residual/NO_y statistical distribution, or some of the variance observed in previous airborne intercomparison studies (see earlier discussion in sections 2.1-2.3 and *Gregory et al.* [1990 *c*, *d*]). However, as far as the clearly out-of-balance data are concerned, it is difficult for us to explain this magnitude of budget deficit on the subtle sampling problems discussed above. In addition, it is difficult to understand how such effects would retain an on average tendency for correlation with O_3, PAN, and temperature.

The catalytic conversion of N_2O, X-NH, and X-CN compounds is believed to be small based on laboratory test. However, exhaustive tests have not been carried out using the wide range of possible conditions and chemical mixtures encountered throughout the troposphere. If catalytic conversion of these types of compounds did occur, then another possible explanation for the apparent NO_y

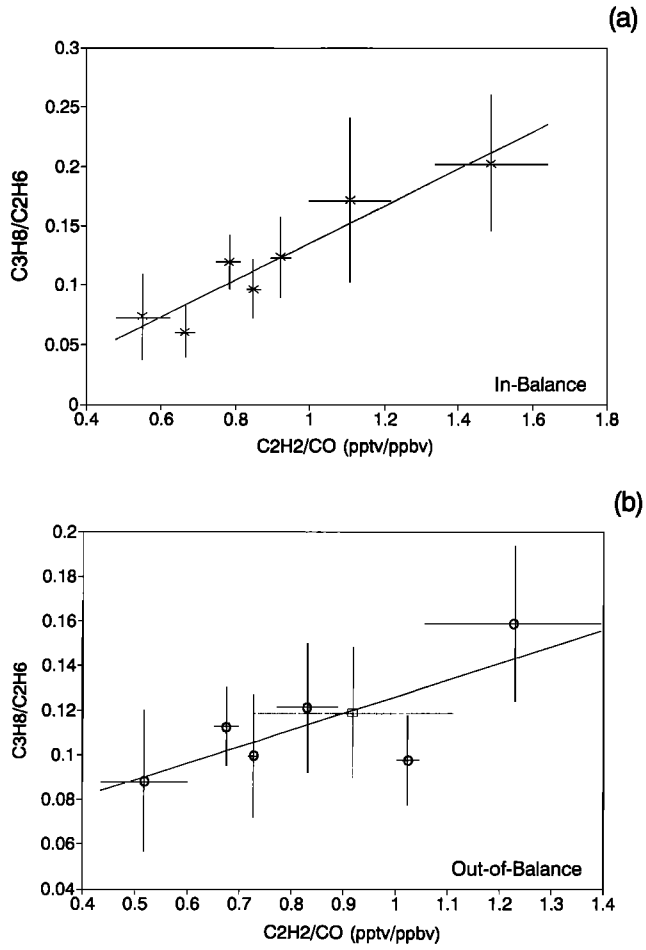

Fig. 15. Graphs of aggregated data for C_3H_8/C_2H_6 versus C_2H_2/CO: (*a*) in balance (cross) (slope 0.156 ±0.023 with r^2 = 0.90) and (*b*) out of balance (circle) (slope = 0.074 ±0.033 with r^2 = 0.56). Horizontal and vertical bars as in Figure 9.

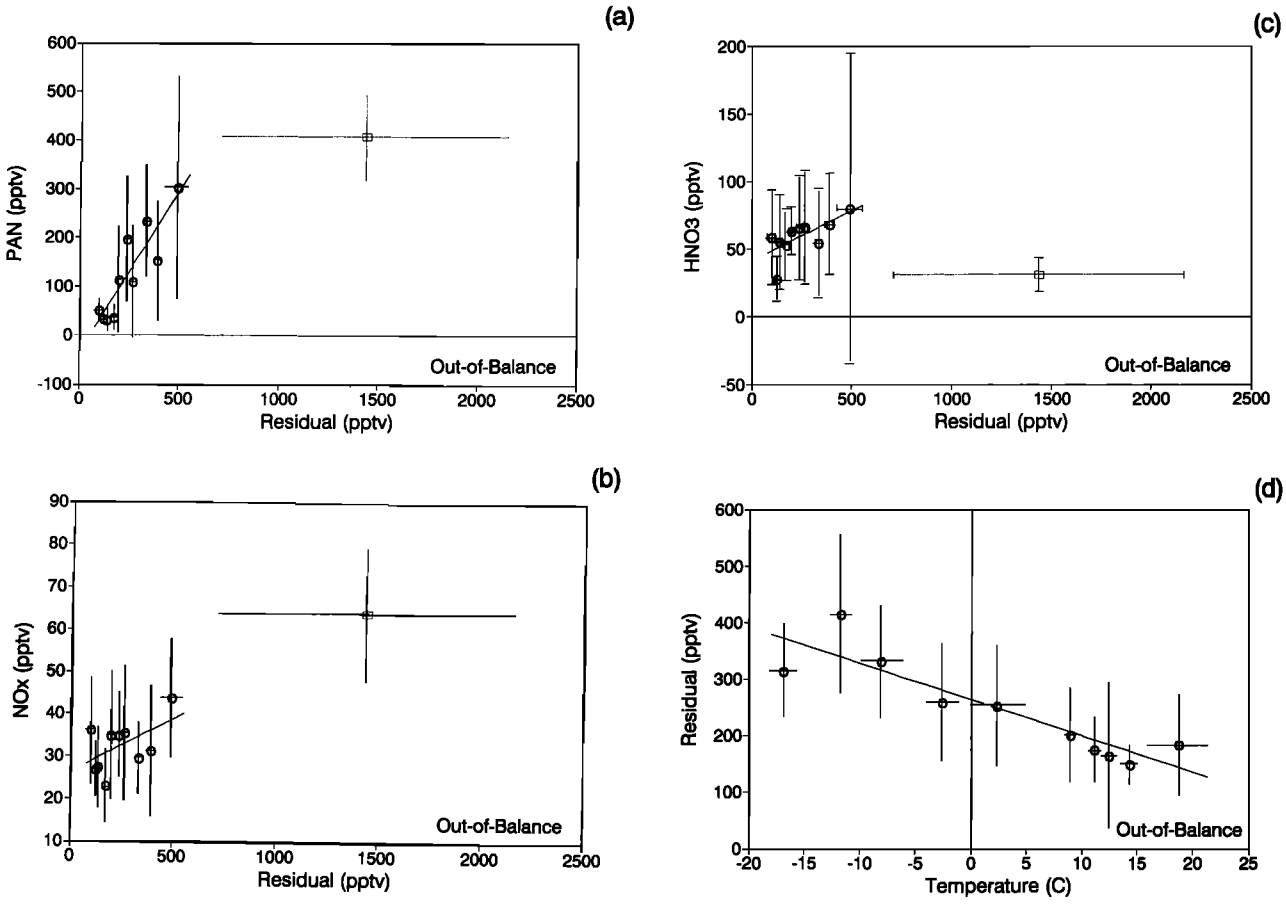

Fig. 16. Graphs of aggregated out of balance data for (*a*) PAN versus residual (slope = 0.658 ±0.123 with r^2 = 0.78); (*b*) NO_x versus residual (slope = 0.025 ±0.014 with r^2 = 0.29); (*c*) HNO_3 versus residual (slope = 0.074 ±0.028 with r^2 = 0.47); and (*d*) residual vs temperature for nonplume data only (slope = -6.4 ±1.1 with r^2 = 0.81). Horizontal and vertical bars as in Figure 9.

budget deficit might exist. In particular, conversion of compounds such as X-CN or X-NH could also be consistent with the correlative trends in O_3 and PAN, if these compounds became eventually oxidized to produce NO_x. Biomass burning, which impacted all of the ABLE-3 study regions, has been shown to produce X-CN compounds [*Lobert et al.*, 1990]. Therefore this, speculation, that of X-CN compounds, could also be consistent with the ABLE 3A ground-based NO_y measurement results. The concurrent ground-based NO_y, HNO_3, and NO_x measurements in the ABLE 3A program showed good agreement in both the magnitude and the partitioning of NO_y with the lowest altitude (~ 0.15 km) measurements taken on the aircraft [*Bakwin et al.*, 1992]. They attributed nearly half of the ground-based measured NO_y to "missing" compounds (~100 pptv) and very little to the labile compound PAN. Their tower flux measurements also indicated that these missing compounds also exhibited a small deposition velocity (i.e., sixfold smaller than O_3). This would suggest that the missing NO_y compounds in the lower-altitude range are relatively unreactive. Subtle changes in the catalytic convertor Au-surface's condition might significantly reduce the conversion efficiency for these more difficult to convert compounds (i.e., X-CN) without producing a noticeable change in the conversion efficiency of reducible compounds such as HNO_3, NO_2, or PAN. This type of mechanism could possibly explain the observed shift in NO_y budget trends for the predominantly in-balance northern Labrador/Quebec data. This hypothesis would also be consistent with the suggestions that some portion of the NO_y budget deficit is comprised of relatively unreactive nitrogen-containing compounds. The above hypothesis suggests that more detailed conversion efficiency tests need to be carried out under a wide range of conditions for a number of compounds.

4. SUMMARY

The summertime partitioning and budget of tropospheric N_xO_y compounds have been investigated in the middle to lower troposphere over three high-latitude regions of North America. These investigations are the first to use a spectroscopically selective measurement system to detect the NO produced from a NO_y Au-catalytic converter. The N_xO_y budget was analyzed for the degree of closure based on the balance obtained from comparing observed NO_y

mixing ratios to the sum of individual $NO_y(i)$ species (NO_x, HNO_3, PAN, and PPN). Within the estimated precision and accuracy of the measurements, statistically significant differences were found between the ABLE 3 study regions.

In the middle free troposphere (3 - 6 km) over Alaska and the Hudson Bay lowlands, approximately 73% of the analyzed measurements indicate a deficit in the NO_y budget at the 95% confidence limit. The NO_y budget within the lower altitudes (0.15 - 3 km) also had a deficit. In these cases, approximately 87% of the Alaska and 35% of the Hudson Bay lowland measurements indicate a deficit at the 95% confidence limit.

Over the northern Labrador/Quebec region the NO_y budget was more completely accounted for by the measured $NO_y(i)$ species. In this case, approximately 83% of the analyzed measurements fall inside the 95% confidence interval, with a nearly equal distribution about zero of residual values defined by $NO_y - \Sigma NO_y(i)$. A combination of measurement uncertainty and poor temporal overlap between the various $NO_y(i)$ measurements is indicated as the dominant causes limiting our ability to assess the degree of closure within the NO_y budget at values of $\Sigma NO_y(i)/NO_y$ greater than about 0.6. This result is similar to that observed in other NO_y to $\Sigma NO_y(i)$ budget studies [e.g., *Parrish et al.*, 1993]. Where the improved level of uncertainty that has recently been observed at two of the ground-based rural locations is perhaps not unexpected when the larger NO_y mixing ratios and larger fraction of more reliably measured NO_x are taken into account, along with the more slowly changing atmospheric conditions found at ground-sites.

The large deficit in the NO_y budget (having $\Sigma NO_y(i)/NO_y < 0.6$) over regions of Alaska and the Hudson Bay lowlands appears to be related to factors that influence the oxidative potential of the troposphere over these regions as reflected by the mixing ratios of O_3. Based on our discussion of possible measurement errors and the correlative tendencies exhibited with other compounds, it is unlikely that the bulk of this NO_y budget deficit is due to a simple artifact of the measurements. A portion of this NO_y budget deficit is also suggested to be in the form of relatively unreactive nitrogen-containing compounds, especially at the lower altitudes. However, based on the correlations with O_3 and temperature, a larger fraction of the implied NO_y budget's missing compounds exhibit trends that are more indicative of the labile NO_x-reservoir PAN. This could suggest that these missing compounds either have chemical characteristics that are similar to PAN or that they have a similar atmospheric source as PAN.

Acknowledgments. The authors would like to thank Roger Navarro, Dave Pierce, and the flight and ground crews of the Wallops Island Electra for their endeavors to make the operation a safe and successful one. We would like to thank our Canadian hosts for their friendly and cordial hospitality during the field campaign. A special thanks to Jim Hoell, Richard Bendura, Helen Thompson, and Yolanda Dennis for their perseverance in making and maintaining logistical arrangements throughout all of ABLE 3B. The investigators at Georgia Tech would like to thank Gerhard Hübler for his helpful suggestion and comments on the development of their NO_y system and for providing the authors with preprints of his manuscripts. We also appreciate helpful discussions with Shaw Liu, Stewart McKeen, and Dave Fahey, and the helpful suggestions from our two anonymous reviewers. We would also like to acknowledge the contributions of Sandra Farber and Ding-Jun Yang toward the preparation of this manuscript. This research was sponsored by the National Aeronautics and Space Administration, Tropospheric Chemistry Program.

References

Anderson, B. E., G. L. Gregory, J. D. W. Barrick, J. E. Collins, G. W. Sachse, M. C. Shipham, and C. H. Hudgins, Summertime tropospheric ozone distributions over central and eastern Canada, *J. Geophys. Res.*, this issue.

Atlas, E. L., B. A. Ridley, G. Hübler, J. G. Walega, M. A. Carroll, D. D. Montzka, B. J. Huebert, R. B. Norton, F. E. Grahek, and S. Schauffler, Partitioning and budget of NO_y species during MLOPEX, *J. Geophys. Res.*, *97*, 10,449-10,462, 1992.

Bakwin, P. S., S. C. Wofsy, and S. M. Fan, Measurements of NO_x and NO_y concentrations and fluxes over Arctic tundra, *J. Geophys. Res.*, *97*, 16,545-16,557, 1992.

Blake, D. R., D. F. Hurst, T. W. Smith, Jr., W. J. Whipple, T. Y. Chen, N. J. Blake, and F. S. Rowland, Summertime measurements of selected nonmethane hydrocarbons in the Arctic and subarctic in 1988 during the 1988 Arctic Boundary Layer Expedition (ABLE) 3A, *J. Geophys. Res.*, *97*, 16,559-16,588, 1992.

Blake, D. R., T. W. Smith, Jr., T. Y. Chen, W. J. Whipple, and F. S. Rowland, Effects of biomass burning on summertime nonmethane hydrocarbon concentrations in the Canadian wetlands, *J. Geophys. Res.*, this issue.

Bollinger, M. J., R. F. Sievers, D. W. Fahey, and F. C. Fehsenfeld, Conversion of nitrogen dioxide, nitric acid, and n-propyl nitrate to nitric oxide by gold catalyzed reduction with carbon monoxide, *Anal. Chem.*, *55*, 1980-1986, 1983.

Bradshaw, J. D., M. O. Rodgers, S. T. Sandholm, S. Kesheng, and D. D. Davis, A two-photon laser-induced fluorescence field instrument for ground-based and airborne measurements of atmospheric NO, *J. Geophys. Res.*, *90*, 12,861-12,873, 1985.

Browell, E. V., M. A. Fenn, C. F. Butler, W. B. Grant, R. C. Harriss, and M. C. Shipham, Ozone and aerosol distributions in the summertime troposphere over Canada, *J. Geophys. Res.*, this issue.

Buhr, M. P., D. D. Parrish, R. B. Norton, F. C. Fehsenfeld, and R. E. Sievers, Contribution of organic nitrates to the total reactive nitrogen budget at a rural eastern U.S. site, *J. Geophys. Res.*, *95*, 9,809-9,816, 1990.

Carroll, M. A., et al., Aircraft measurements of NO_x over the eastern Pacific and continental United States and implications for ozone production, *J. Geophys. Res.*, *95*, 10,205-10,233, 1990.

Chameides, W. L., D. D. Davis, M. O. Rodgers, J. Bradshaw, S. Sandholm, G. Sachse, G. Hill, G. Gregory, and R. Rasmussen, Net ozone photochemical production over the eastern and central North Pacific as inferred from GTE/CITE 1 observations during fall 1983, *J. Geophys. Res.*, *92*, 2,131-2,152, 1987.

Chameides, W. L., et al., Ozone precursor relationships in the ambient atmosphere, *J. Geophys. Res.*, *97*, 6,037-6,055, 1992.

Crutzen, P. J., The role of NO and NO_2 in the chemistry of the troposphere and stratosphere, *Ann. Rev. Earth Planet. Sci.*, *7*, 443-472, 1979.

DeMore, W. B., S. P. Sander, M. J. Molina, D. M. Golden, R. F. Hampson, M. J. Kurylo, C. J. Howard, and A. R. Ravishankara, Chemical kinetics and photochemical data for use in stratospheric modeling, in *Evaluation 10, JPL Publ. 90-91*, Jet Propul. Lab., Pasadena Calif., 1992.

Fahey, D. W., C. S. Eubanks, G. Hübler, and F. C. Fehsenfeld, Evaluation of a catalytic reduction technique for the measurement of total reactive odd-nitrogen NO_y in the atmosphere, *J. Atmos. Chem.*, *3*, 435-468, 1985.

Fahey, D. W., G. Hübler, D. D. Parrish, E. J. Williams, R. B. Norton, B. A. Ridley, H. B. Singh, S. C. Liu, and F. C. Fehsenfeld, Reactive nitrogen species in the troposphere: Measurements of NO, NO_2, HNO_3, particulate nitrate, peroxyacetyl nitrate (PAN), O_3, and total reactive odd nitrogen (NO_y) at Niwot Ridge, Colorado, *J. Geophys. Res.*, *91*, 9781-9793, 1986.

Gaffney, J. S., R. Fajer, and G. L. Senum, An improved procedure for high purity gaseous peroxyacetyl nitrate production: Use of heavy

lipid solvents, *Atmos. Environ., 18,* 215-218, 1984.

Gregory, G. L., C. H. Hudgins, and R. A. Edahl, Laboratory evaluation of an airborne ozone instrument which compensates for altitude/sensitivity effects, *Environ. Sci. Technol., 17,* 100-103, 1983.

Gregory, G. L., J. M. Hoell, Jr., A. L. Torres, M. A. Carroll, B. A. Ridley, M. O. Rodgers, J. D. Bradshaw, S. T. Sandholm, and D. D. Davis, An intercomparison of airborne nitric oxide measurements: A second opportunity, *J. Geophys. Res., 95,* 10129-10138, 1990*a*.

Gregory, G. L., et. al., An intercomparison of airborne nitrogen dioxide instruments, *J. Geophys. Res., 95,* 10, 103-10, 127, 1990*b*.

Gregory, G. L., J. M. Hoell, Jr., B. A. Ridley, H. B. Singh, B. Gandrud, L. J. Salas, and J. Shetter, An intercomparison of airborne PAN measurements, *J. Geophys. Res., 95,* 10,077-10,087, 1990*c*.

Gregory, G. L., et al., An intercomparison of airborne nitric acid measurements, *J. Geophys. Res., 95,* 10,089-10,102, 1990*d*.

Harriss, R. C., et al., The Arctic Boundary Layer Expedition (ABLE) 3A: July-August 1988, *J. Geophys. Res., 97,* 16,383-16,394, 1992.

Harriss, R. C., S. C. Wofsy, J. M. Hoell, Jr., R. J. Bendura, J. W. Drewry, R. J. McNeal, D. Pierce, V. Rabine, and R. L. Snell, The Arctic Boundary Layer Expedition (ABLE) 3B: July-August 1990, *J. Geophys. Res.,* this issue.

Hoell, J. M., G. L. Gregory, D. S. McDougal, A. L. Torres, D. D. Davis, J. D. Bradshaw, M. O. Rodgers, B. A. Ridley, and M. A. Carroll, Airborne intercomparison of nitric oxide measurement techniques, *J. Geophys. Res., 92,* 1995-2008, 1987.

Hough, A. M., and C. E. Johnson, Modelling the role of nitrogen oxides, hydrocarbons and carbon monoxide in the global formation of tropospheric oxidants, *Atmos. Envir., 25(A),* 1819-1835, 1991.

Hubert, B. J., et al., Measurements of the nitric acid to NO_x ratio in the troposphere, *J. Geophys. Res., 95,* 10,193-10,198, 1990.

Hübler, et al., Total reactive oxidized nitrogen (NO_y) in the remote Pacific troposphere and its correlation with O_3 and CO: MLOPEX 1988, *J. Geophys. Res., 97,* 10,427-10,447, 1992.

Jacob, D. J., et al., Summertime photochemistry of the troposphere at high northern latitudes, *J. Geophys. Res., 97,* 16,421-16,431, 1992.

Lin, X., M. Trainer, and S. C. Liu, On the nonlinearity of the tropospheric ozone production, *J. Geophys. Res., 93,* 15,879-15,888, 1988.

Liu, S. C., M. McFarland, D. Kley, O. Dafiriou, and B. Huebert, Tropospheric NO_x and O_3 budget in the equatorial Pacific, *J. Geophys. Res., 88,* 1360-1368, 1983.

Lobert, J. M., D. H. Scharffe, W.M. Hao, and P.J. Crutzen, Importance of biomass burning in the atmospheric budgets of nitrogen containing gases, Nature, 346, 552 - 554, 1990.

Logan, J. A., M. J. Prather, S. C. Wofsy, and M. B. McElroy, Tropospheric chemistry: A global perspective, *J. Geophys. Res., 86,* 7,210-7,254, 1981.

Logan, J. A., Nitrogen oxides in the troposphere: Global and regional budgets, *J. Geophys. Res., 88,* 10,785-10,807, 1983.

Murphy, D. M., and D. W. Fahey, Mathematical treatment of the wall loss of a trace species in denuder and catalytic converter tubes, *Anal. Chem., 59,* 2753-2759, 1987.

Parrish, D. D., M. Trainer, M. P. Buhr, B. A. Watkins, and F. C. Fehsenfeld, Carbon monoxide concentrations and their relation to concentrations of total reactive oxidized nitrogen at two rural U. S. sites, *J. Geophys. Res., 96,* 9309-9320, 1991.

Parrish, D. D., et al., The total reactive oxidized nitrogen levels and the partitioning between the individual species at six rural sites in eastern North America, *J. Geophys. Res., 98,* 2927-2939, 1993.

Ridley, B. A., Recent measurements of oxidized nitrogen compounds in the troposphere, *Atmos. Environ., 25,* 1905-1926, 1991.

Roberts, J. M., The atmospheric chemistry of organic nitrates, *Atmos. Environ., 24(A),* 243-287, 1990.

Sachse, G. W., G. F. Hill, L. O. Wade, and M. G. Perry, Fast response, high-precision carbon monoxide sensor using a tunable diode laser absorption technique, *J. Geophys. Res., 92,* 2071-2081, 1987.

Sandholm, S. T., J. D. Bradshaw, K. S. Dorriss, M. O. Rogers, and D. D. Davis, An airborne compatible photofragmentation two-photon laser-induced fluorescence instrument for measuring background tropospheric NO, NO_x, and NO_2, *J. Geophys. Res., 95,* 10,155-10,161, 1990.

Sandholm, S. T., J. D. Bradshaw, G. Chen, H. B. Singh, R. W. Talbot, G. L. Gregory, D. R. Blake, G. W. Sachse, E. V. Browell, J. D. Barrick, M. A. Shipham, A. S. Bachmeier, and D. Owen, Summertime tropospheric observations related to N_xO_y distributions and partitioning over Alaska: Artic Boundary Layer Expedition (ABLE) 3A, *J. Geophys. Res., 97,* 16,481-16,509, 1992.

Shipham, M. C., A. S. Bachmeier, D. R. Cahoon, Jr., and E. V. Browell, Meteorological overview of the ABLE 3B flight series, *J. Geophys. Res., 97,* 16,395-16,419, 1992.

Shipham, M. C., A. S. Bachmeier, D. R. Cahoon, G. L. Gregory, and B. E. Anderson, E. V. Browell, Meteorological interpretation of the Arctic Boundary Layer Expedition (ABLE) 3B flight series, *J. Geophys. Res.,* this issue.

Singh, H. B., Reactive nitrogen in the troposphere, *Environ. Sci. Technol., 21,* 320-327, 1987.

Singh, H. B., and P. L. Hanst, Peroxyacetyl nitrate (PAN) in the unpolluted troposphere: An important reservoir for nitrogen oxides, *Geophys. Res. Lett., 8,* 941-944, 1981.

Singh, H. B., and L. J. Salas, Methodology for the analyses of peroxyacetyl nitrate (PAN) in the unpolluted atmosphere, *Atmos. Environ., 17,* 1507-1516, 1983.

Singh, H. B., et al., PAN measurements during CITE 2: Atmospheric distribution and precursor relationships, *J. Geophys. Res., 95,* 10,163-10,178, 1990.

Singh, H. B., D. O'Hara, D. Herlth, J. D. Bradshaw, S. T. Sandholm, G. L. Gregory, G. W. Sachse, and D. R. Blake, Atmospheric measurements of PAN and other organic nitrates at high latitudes: Possible sources and sinks, *J. Geophys. Res., 97,* 16,511 - 16,522, 1992a.

Singh, H. B., D. Herlth, K. Zahnle, D. O'Hara, J. D. Bradshaw, S. T. Sandholm, R. Talbot, P. J. Crutzen, and M. Kanakidou, Relationships of PAN to active and total odd nitrogen at northern high latitudes: Influence of reservoir species on NO_x and O_3, *J. Geophys. Res., 97,* 16,523 -16,530, 1992*b*.

Singh, H. B., et al., Summertime Distribution of PAN and other reactive nitrogen species in the northern high-latitude atmosphere of eastern Canada, *J. Geophsy. Res.,* this issue.

Talbot, R. W., A. S. Vijgen, and R. C. Harriss, Measuring tropospheric HNO_3: Problems and prospects for nylon filter and mist chamber techniques, *J. Geophys. Res., 95,* 7553-7561, 1990.

Talbot, R. W., A. S. Vijgen, and R. C. Harriss, Soluble species in the Arctic summer troposphere: Acidic gases, aerosols, and precipitation, *J. Geophys. Res., 97,* 16,531 - 16.543, 1992.

Talbot, R. W., et al., Summertime Distribution and relations of reactive odd nitrogen species and NO_y in the troposphere over Canada, *J. Geophys. Res.*, this issue.

Wofsy, S. C., et al., Atmospheric chemistry in the Arctic and subarctic: Influence of natural fires, industrial emissions, and stratospheric inputs, *J. Geophys. Res., 97,* 16,731-16,746, 1992.

Wofsy, S. C., S. M. Fan, D. R. Blake, J. D. Bradshaw, S. T. Sandholm, H. B. Singh, G. W. Sachse, and R. C. Harriss, Factors influencing atmospheric conditions composition over subarctic North America during summer, *J. Geophys. Res.,* this issue.

B. Anderson, J. Barrick, J. Collins, G. Gregory, and G. Sachse, NASA Langley Research Center, Hampton, VA 23665.

D. Blake, Department of Chemistry, University of California at Irvine, Irvine, CA 92717.

J. Bradshaw, J. Olson, S. Sandholm, School of Earth and Atmospheric Sciences, Georgia Institute of Technology, Atlanta, GA 30332.

K. Gorzelska, B. Lefer, and R. Talbot, Institute for the Study of Earth, Oceans, and Space, University of New Hampshire, Durham, NH 03824.

D. Herlth, D. O'Hara, and H. Singh, NASA Ames Research Center, Moffett Field, CA 94035.

K. Klemm and O. Klemm, Now at Fraunhofer-Institut für Atmosphärische Umweltforschung, Garmisch-Partenkirchen, Germany.

(Received August 12, 1992; revised August 7, 1993;
accepted August 25, 1993.)